VELOCITY MEASUREMENT OF LASER ENERGY INDUCED RAYLEIGH SURFACE WAVES ON BULK SUBSTRATES EMPLOYING THE OPTICAL BEAM DEFLECTION (KNIFE-EDGE DETECTION) METHOD

by

Timothy S. Glenn

S. B., Aeronautical and Astronautical Engineering
Massachusetts Institute of Technology, 1993

Submitted to the Department of Aeronautics and Astronautics
in Partial Fulfillment of the Degree of

MASTER OF SCIENCE

at the

MASSACHUSETTS INSTITUTE OF TECHNOLOGY

June 1995

Signature of Author .....
Department of Aeronautics and Astronautics
May 12, 1995

Certified by .....
Professor Nesbitt W. Hagood, IV
Thesis Supervisor

Certified by .....
Dr. Dick J. Chang
The Aerospace Corporation
Company Supervisor

Accepted by .....
Professor Harold Y. Wachman
Chairman, Department Graduate Committee

VELOCITY MEASUREMENT OF LASER ENERGY INDUCED RAYLEIGH SURFACE WAVES ON BULK MATERIAL SUBSTRATES EMPLOYING THE OPTICAL BEAM DEFLECTION (KNIFE-EDGE DETECTION) METHOD

by

TIMOTHY S. GLENN

Submitted to the Department of Aeronautics and Astronautics
on May 12, 1995 in Partial Fulfillment of the
Requirements for the Degree of Master of Science
at the Massachusetts Institute of Technology

ABSTRACT

Rayleigh surface wave velocities of several bulk material substrates were accurately measured using a system of lasers for both generation and detection. In most cases, the neodymium:YAG pulse laser used to excite the waves successfully generated them thermoelastically and without damage to the surface. This was made possible by line-focusing the beam with a cylindrical lens which directed the energy of the acoustic source in the direction of the detection probe. The helium-neon laser used to observe the propagation of the surface waves was configured using an optical beam deflection/knife-edge detection scheme and employed a micropositioning translation stage to accurately measure relative distances with a precision of $\pm 2.5\ \mu m$.

The experimental velocity results agreed with published values to well within 1%, demonstrating the validity of the technique. Also the results were extremely reproducible within a range of approximately 0.2%. The precision of this technique was generally limited by the resolution of the digitally captured oscilloscope traces.

Conclusions are made regarding future adaptation of this technique for use on thin films to measure their elastic constants.

Thesis Supervisor:
Prof. Nesbitt W. Hagood
Dept. of Aeronautics and Astronautics

Company Supervisor:
Dr. Dick J. Chang
The Aerospace Corporation

ACKNOWLEDGMENTS

Funding for this research was provided to The Aerospace Corp. by the Aerospace and Material Sciences Directorate of the Air Force Office of Scientific Research (AFOSR), Bolling Air Force Base, Washington DC, 20332, where Dr. Walter F. Jones is Program Manager, and Dr. Jim C. I. Chang is Director.

Great thanks go to my supervisor, Dr. Dick J. Chang, who supported me throughout my stay as an intern at The Aerospace Corp. He was always very clear as to what was expected of me and always made my transitions into and out of stays at the company very comfortable. I also greatly appreciate the support of Dr. Munson Kwok, Department Director, and his efforts to keep the company's interest in the internship program alive.

TABLE OF CONTENTS

LIST OF FIGURES

LIST OF TABLES

1 INTRODUCTION

The existence of elastic waves which travel in a thin layer adjacent to the free surface of a solid has been known for a long time.[1] While initially of interest mainly to seismologists, these surface waves became important for such technical applications as surface flaw detection with the development of methods for generating them piezoelectrically.[2] In this work, a system of excitation and detection lasers was investigated to accurately measure the velocities of Rayleigh surface waves on bulk material samples. Laser ultrasonics is a relatively new field, but with promises of surmounting many of the limitations associated with piezoelectric transduction, interest in it is quickly growing. Here, lasers were hoped to provide a remote, nondestructive method of characterizing material properties, particularly the elastic modulus, an objective which might not necessarily be fully realizable with piezoelectrics.

The main focus of the optics laboratory at The Aerospace Corp. in which this research was accomplished lies in laser-based measurement systems, providing the decisive influence toward the use of lasers, as opposed to the more customary techniques used in ultrasonics including piezoelectric transducers. Rayleigh surface wave velocity experiments have been carried out using these other methods, but as was just mentioned and will be discussed in detail, lasers may provide a promising, if not superior alternative.

1. Lord Rayleigh, Scientific Papers (Cambridge at the University Press, 1900), Vol. 2, p. 441.
2. F. Firestone and I. Frederick, *J. Acoustic Soc. Am.* **18**, 200 (1946).

Note that the experimental method discussed in this thesis has been tested only on bulk material substrates, both isotropic and cubic crystalline, with future considerations to adapting the technique to thin films.

1.1 Objective

The original objective of the research discussed in this paper was directed toward investigating the use of lasers in developing a method for determining the elastic modulus of thin films, for their mechanical properties such as the elastic modulus are in great demand to assess the reliability of thin film coated components. Whether an engineer endeavors to analytically determine the residual stresses incurred during the deposition process or to predict the effects of radiation, he must know the film's properties with reasonable certainty to achieve an accurate theoretical analysis.

A more attainable objective, however, fashioned itself into investigating a method which, through further study, could conceivably be adapted for use on thin films, but, as an initial step in the right direction, could presently be tested on bulk material samples, both isotropic and crystalline. The chosen method would need to take into consideration the extreme nature of thin films; leaving the film intact, i.e. still deposited on its substrate, and searching for an indirect method to measure the elastic modulus became a fundamental requirement. This initiated the development of a system of lasers to generate and detect Rayleigh surface waves, the velocity of which is a function of the material properties, including the elastic modulus. In turn, the focus of this research was tailored to the study of a particular technique of employing lasers to accurately measure the velocity of these Rayleigh waves, or equivalently, the elastic modulus of the traveling medium.

The resulting experimental procedure involved exciting a surface wave with a single, high-energy pulse of a Q-switched neodymium-yttrium-aluminum-garnet (Nd:YAG) infrared laser. The propagation of the surface transient was then observed by an independent continuous wave (cw) helium-neon (He-Ne) laser probe at a distance from the exci-

tation spot. This detection laser system was configured using an optical beam deflection (knife-edge detection) technique, and the velocity was extrapolated using signal processing software. The resulting problem was defined as follows: investigate the overall worth of the laser method, especially the accuracy with which it measures the surface wave velocity, when applied to bulk substrates, and propose possible ways to apply what is gained by this research to the improved reliability assessment of thin films.

1.2 Motivation

In the present age, any practicing engineer has ready access to the physical and mechanical properties of almost every common material needed to complete an accurate analysis. But some configurations of even the simplest of materials can lead to very complex structural and thermal analyses. Some, like composites, have spawned new advancements in the area of complex materials theory. Still, though, the material constants of most composite materials are readily known beforehand leaving the bulk of the problem to the analysis.

The difficulty with thin films is the reverse. Very often the theoretical analysis is well defined, but the material properties are not. They can differ significantly from the known bulk material constants due to deposition induced anisotropies and other such considerations which are much too involved to get into in this discussion. It is only important to note here that materials used in thin films can behave differently as films then when in bulk form.

In optical systems thin films are widely used as coatings on mirrors, lenses, and collimator benches. Other applications include oxidation retardation, thermal control, and dry lubrication. In these applications, the structural and thermal stress gradients within the film can be very large. The extreme conditions under which a given film will last can be crucial to know in advance, leaving it to theory to predict the results. This requires prior

knowledge of the mechanical properties of the films, the goal to which the research carried out in this paper aims to supply a functional building block.

The point is thin film mechanical properties are not readily available or accurately determinable using conventional methods. Direct stress-strain testing is very difficult to perform on extremely delicate, etched-away, stand-alone films, and the error is likely to be unacceptable. Therefore, a new and innovative method is essential to the advancement of theoretical thin film analysis and reliability assessment.

2 BACKGROUND

Undeniably, several experimental methods exist that were developed solely to measure the mechanical properties of thin films, and others that have the potential to be adapted to do the same. Two such techniques include 1) the cantilever resonance method[1] and 2) surface ultrasonics via piezoelectric transduction or acoustic microscopy. The former was investigated at The Aerospace Corp. and is an example of a method which is explicitly designed for measuring the modulus of thin films. The latter is a general classification of techniques based on the ultrasonic generation and detection of surface waves. Though considerable efforts have been made to study surface waves in bulk materials using these techniques, very little work has been done regarding surface waves travelling in thin films where the penetration depth becomes much more of an issue. Overcoming that one problem, which will be discussed in detail in Chapter 3, could open the doors for surface wave analysis on thin films.

2.1 Cantilever Resonance Method

The method. The cantilever resonance method is a simple concept governed by the equations of a layered beam. It compares the resonant frequency of a cantilevered substrate before and after film deposition to determine the Young's modulus of the film. For small thickness ratios, i.e. for $d_f/d_s \ll 1$, the relation is given by the equation

1. D. J. Chang, R. Muki, P. M. Adams, K. W. Paschen, and C. Tseng, "Thin Film-Residual Stress Assessment." SD-TR-88-28, The Aerospace Corp., 1988.

$$\frac{E_f}{E_s} = \frac{1}{3}\left[\frac{2\,(f - f_0)}{f_0} \cdot \frac{d_s}{d_f} + \frac{\rho_f}{\rho_s}\right], \tag{2-1}$$

where E is Young's modulus, d is thickness, ρ is density, and the subscripts f and s signify film and substrate. The measurable quantities are the bare substrate's resonant frequency, f_0, and the resonant frequency, f, of the specimen with the deposited film. From these two frequencies, the film's modulus can be calculated. (Figure 2-1 illustrates the experimental apparatus used at The Aerospace Corp.)

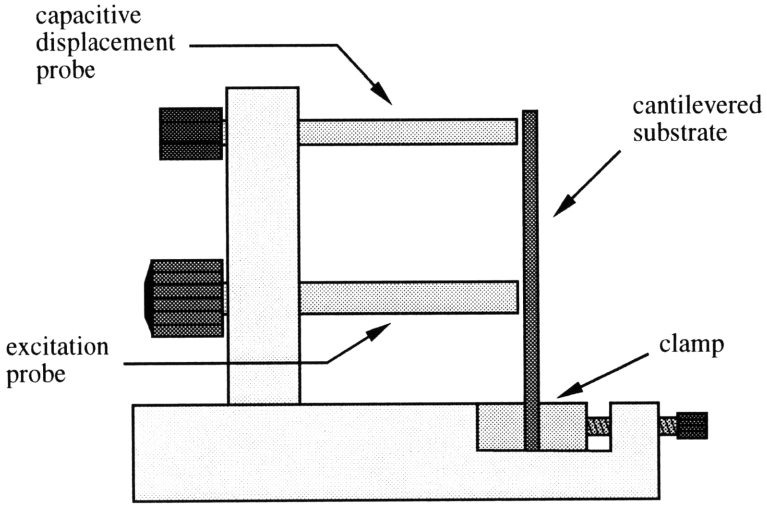

FIG. 2-1. Cantilever resonance method.

Problems. One of the major disadvantages of this method is that it cannot be used to test an arbitrary sample, for each specimen must be cut with exact precision for the calculation to be at all accurate. Thus, the method is worthless to an engineer who wishes to analyze a prefabricated thin film coated component, which could often be the case if he offers outside customer support. Not only must the specimen have a simple geometry, but the procedure also requires the testing of it before and after film deposition. Also, a non-uni-

form film thickness could greatly skew the results because the film properties are not measured locally, but, rather, they are averaged over the entire sample.

The above disadvantages are more often dwarfed by the questionable accuracy and repeatability of the technique. The lines of constant density ratio in Figure 2-2[1] demonstrate how extremely sensitive the calculated modulus ratio is to errors in the measured frequency ratio. Their slope is proportional to d_f/d_s, so typically a thin substrate is required to provide a sensitive $(f-f_0)/f_0$ value, but there are practical limits to the manufacturing of the substrate. For the substrate thickness ratio given in the figure, a frequency measurement error of only one part in ten thousand, which was typical in the measurements compiled at The Aerospace Corp., leads to errors in the modulus calculation on the order of six percent.

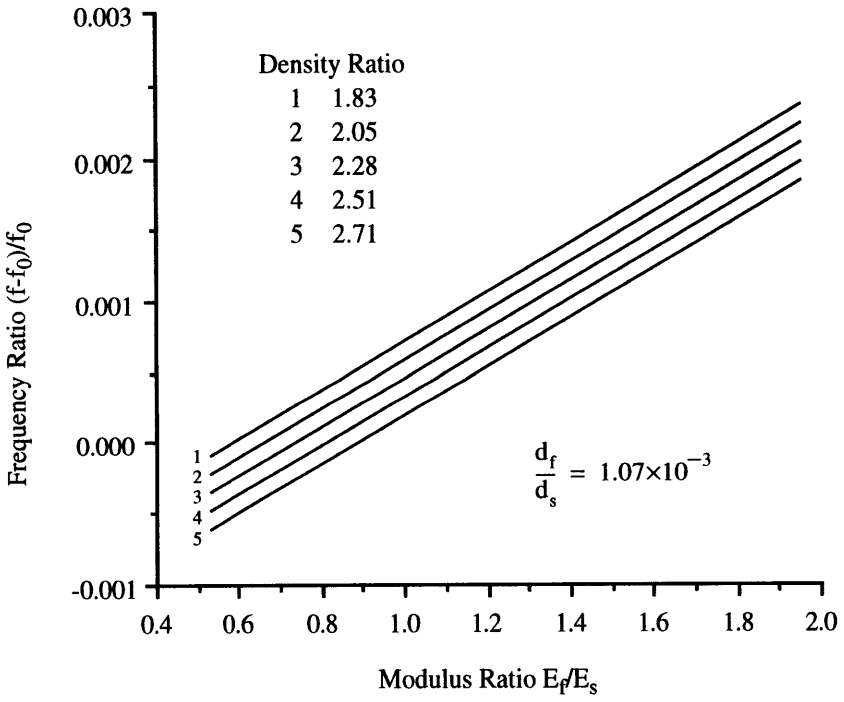

FIG. 2-2. Frequency ratio vs. modulus ratio for $d_f/d_s = 1.07 \times 10^{-3}$.

1. Chang *et al.*, p. 63.

Just as important is the lack of acceptable repeatability of the technique. The method in which the sample is placed in the clamping device again and again for each successive test leaves excessive room for measurement error. Not only is the clamped beam not an ideal cantilever, but each time the sample is set into the clamping device, it rests slightly different, thus giving dramatically different frequency readings.

Unfortunately, measurement of the substrate modulus alone leads to errors on the order of 10%, meaning that the error associated with measuring the thin film modulus would be even larger. In theory, the method provides an ideal solution, but in practice it is not so promising. Many of these problematic issues (accuracy, repeatability, range of application, etc.) were addressed and greatly improved by the laser ultrasonics method proposed in this thesis.

2.2 Surface Ultrasonics

Numerous ultrasonics investigators have shown that a material's mechanical properties can be calculated from the velocity of waves travelling through the bulk or on the surface of the material specimen. It naturally follows that, in theory, the elastic modulus of a deposited thin film can be indirectly measured by observing the speed of surface waves on the film. However, in order to discern the properties of only the film using the velocity measurement from a single given specimen, it is important that the energy of the waves exists within a depth less than the thickness of the film. Otherwise the velocity of surface waves is governed by an aggregate sum of the properties of both the film and the substrate. This depth is usually determined by the wavelength of the propagating wave, so application to thin films would require surface waves excited at gigahertz frequencies. This point will be expounded upon later, so for now the discussion will focus on examining traditional and innovative methods of launching and detecting Rayleigh surface waves piezoelectrically.

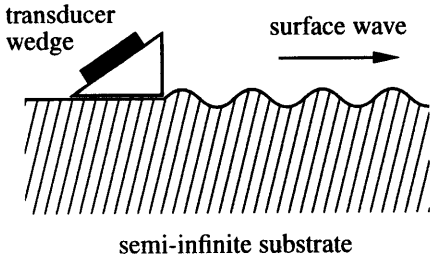

FIG. 2-3. Transducer wedge method for generating Rayleigh surface waves.

2.2.1 Piezoelectric transducers

Surface waves of the Rayleigh type may be generated by placing either an X-cut quartz plate or a Y-cut plate on the surface of a specimen. Some of the energy radiated by the plates is converted into Rayleigh waves but the efficiency is not very high. A method that has been more widely used is the wedge method in which an X-cut quartz thickness plate radiates into a wedge of suitable material (often plastic) placed on the surface, as shown in Figure 2-3. The angle of incidence of the longitudinal waves from the quartz plate, ϕ_1, is chosen so that the angle of refraction, ϕ_2, is 90°. Then

$$\sin\phi_1 = \frac{v_l}{v_R} \tag{2-2}$$

where v_l is the longitudinal wave velocity in the wedge material and v_R is the Rayleigh wave velocity in the object. At this angle it is found that a strong surface wave is propagated in the forward direction only.[1]

A further method that has been used employs an X-cut quartz plate placed on top of an aluminum comb consisting of a set of equidistant teeth and gaps each of width $\lambda_R/2$. The Rayleigh wave generated then has a wavelength of λ_R.[2]

1. H. Sabine and P. H. Cole, "Surface Acoustic Waves in Communications Engineering," *Ultrasonics* **9**, 104 (1971).
2. I. A. Viktorov, "Investigation of Methods for Exciting Rayleigh Waves," *Soviet Physics—Acoustics* **7**, 236 (1962).

More recently, efficient surface wave production has been made possible by the introduction of interdigital electrodes deposited on the surface of a piezoelectric crystal. When an alternating electric field is applied to the fingers of this device, piezoelectric coupling induces a periodic mechanical stress in the crystal which gives rise to a Rayleigh wave. If d is the spacing between neighboring fingers, the frequency of the electric field is chosen so that the Rayleigh wavelength is equal to 2d.[1]

All of the schemes described above are reciprocal, and may operate equally well as either transmitters or receivers of surface waves since the piezoelectric effect works both ways.

2.2.2 Acoustic microscopy

Another approach of using piezoelectrics to measure the velocity of surface waves is reflection mode acoustic microscopy. As shown in Figure 2-4[2], the acoustic microscope consists of a longitudinal wave transducer mounted on a sapphire rod-lens coupled through a liquid (water) to an object surface. The longitudinal waves are focused by the wide angle lens at a distance approximately (4/3)R below the top of the lens where R is its radius. The longitudinal waves reflected from the object surface propagate back to the transducer and produce an output voltage.[3]

The acoustic material signature, V(z), is the variation of the output voltage with distance z from the lens to the object surface in which a series of deep minima of voltage appear at equal intervals. The period of this variation is characteristic of the specimen's elastic material properties involved and results from interference between the two component rays, shown in Figure 2-4, that radiate into the liquid from the solid-liquid interface. As the figure shows, one component is specularly reflected at normal incidence, while the

1. H. F. Pollard, *Sound Waves in Solids* (Pion Limited, London, 1977), p. 202.
2. R. D. Weiglein and A. K. Mal, "Elastic Characterization of Diamond Films by Acoustic Microscopy," unpublished, 4 (1990).
3. W. Parmon and H. L. Bertoni, "Ray Interpretation of the Material Signature in the Acoustic Microscope," *Electron. Lett.* **15**, 684 (1979).

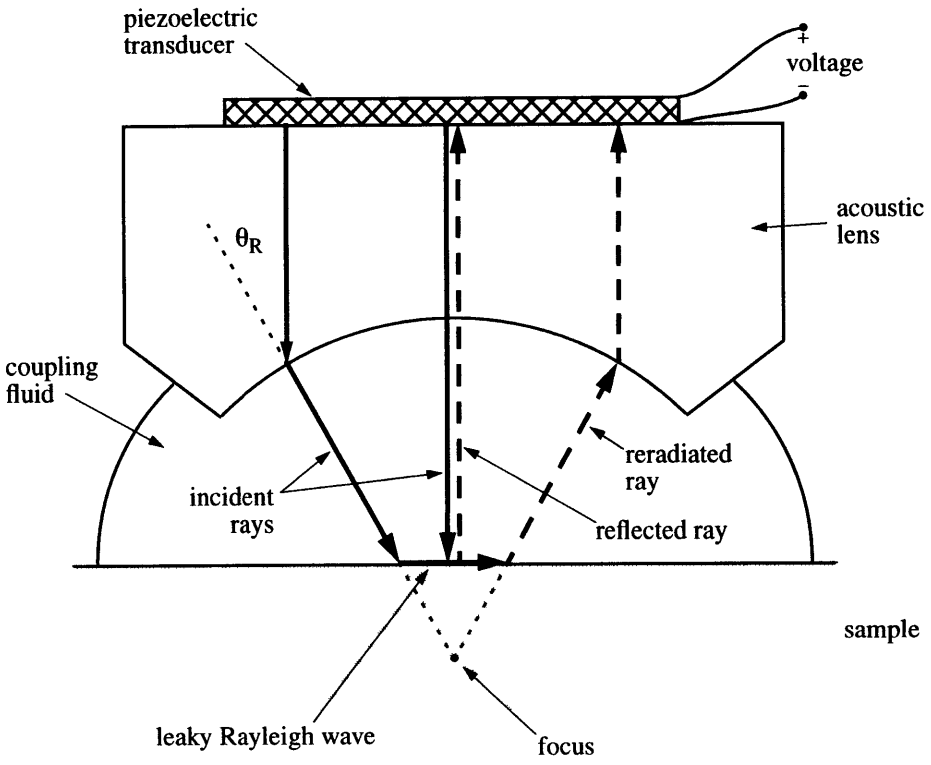

FIG. 2-4. An acoustic microscope probe showing the two dominant ray trajectories. The longitudinal wave incident at the critical Rayleigh angle θ_R excites the leaky Rayleigh wave in the specimen.

second one undergoes a lateral shift on incidence and reradiates at the critical phase-matching angle for Rayleigh waves. The lateral shift is characteristic of a Rayleigh wave that is excited in the specimen and reradiates energy into the liquid at the critical angle. The surface wave velocity can be obtained from the periodic variation of the V(z) curve.[1]

2.2.3 Conclusions

Obviously, the wedge method is impractical owing to the fact that it's geometry requires previous knowledge of the Rayleigh velocity, and since interdigital electrodes require the specimen itself to be piezoelectric, they, too, are not widely practical. But beyond these individual impediments, there exist several global disadvantages to using conventional

1. Weiglein and Mal, p. 4.

piezoelectric transducers in any configuration to measure the Rayleigh velocity accurately and without limitations. The general idea of observing surface waves to characterize thin film elastic properties, though, seems to have considerable potential. Fortunately, many of the problems associated with the use of conventional piezoelectric transducers have been eliminated with the development of optical techniques. The details of this discussion will be expanded upon in the following section with regards to how lasers contribute to resolving them.

2.3 Laser Ultrasonics

Many of the limitations of piezoelectric-based ultrasonics can be traced back to the need for a coupling medium between the transducer and the specimen, so there are considerable benefits to non-contact methods. For example, the contacting nature of piezoelectric techniques introduces inaccuracies owing to variations in coupling efficiency and adds an unknown acoustic impedance, thus hindering the free propagation of waves along the surface of a specimen. Noncontacting methods would allow multiple probes to be projected on the specimen's surface, so that simultaneous data from an array of detectors could be collected without concern for distortions in the acoustic signal resulting from surface loading and other perturbations which would be associated with contacting piezoelectrics.

The main two types of noncontact transduction under current investigation are the electromagnetic acoustic transducer (EMAT)[1] and lasers. EMAT transducers are limited to metals and must be brought in very close proximity to the object surface. Lasers, on the other hand, permit both noncontact and remote generation and detection of surface waves, i.e. the lasers and associated optical components can be sited some distance away from the surface of the specimen. Also, they do not place any requirements on the specimen

1. H. M. Frost, "Electromagnetic-Ultrasound Transducers: Principles, Practice, and applications," in *Physical Acoustics* , W. P. Mason and R. N. Thurston, eds. (Academic Press, New York, 1979), Vol. XIV, p. 179.

for electrical conductivity or magnetic behavior, only that the surface be reflective to some extent to the detection laser's wavelength.

Another concern with conventional techniques is their limited bandwidth at emission and reception. Lasers, on the other hand, involve no mass or structure. They are not governed by mechanical resonance, and as a result, laser techniques can be extremely broadband with a flat frequency response well over several hundred megahertz. The detection bandwidth is usually only limited by the cutoff frequency of the photodetector.[1]

Futhermore, the rise-time of the displacements produced by laser-generated waves can be made comparable to the laser rise-time, which for a Q-switched laser can be of the order of a few nanoseconds, or even picoseconds. This leads to the possibility of undertaking high precision measurements of the velocity of these acoustic modes. Using conventional techniques, the accuracy of absolute velocity measurements is limited to approximately $\pm 0.2\%$ in solids, with the major errors being introduced due to the need for a bond between the sample and the piezoelectric transducer. The removal of this bond, using noncontact laser techniques, potentially leads to an increase in accuracy to a few parts in 10^4 rather than 10^3.[2] This increase in the absolute accuracy of Rayleigh wave velocities in solids would inarguably be important when measuring the elastic properties of thin films or any material.

Pulsed lasers have been used to produce pinpoint acoustic sources which may be scanned over a specimen surface with relative ease. By changing the spatial distribution of the beam, the resulting acoustic signals can be directed and locally intensified.[3] This effect will be achieved later by line focusing the excitation laser beam with a cylindrical lens. Optical detection schemes have been developed which offer similar flexibility in that they

1. J. P. Monchalin, J. D. Aussel, R. Heon, J. F. Bussiere, and P. Bouchard, "Laser-Ultrasonics for Materials Characterization," *Mat. Res. Soc. Symp. Proc.* **142**, 27 (1989).
2. D. A. Hutchins, "Ultrasonic Generation by Pulsed Lasers," in *Physical Acoustics*, W. P. Mason and R. N. Thurston, eds. (Academic Press, New York, 1988), Vol. XVIII, p. 104-105.
3. A. M. Aindow, R. J. Dewhurst, and S. B. Palmer, "Laser Generation of Directional Surface Acoustic Waves Pulses in Metals," *Opt. Commun.* **42**, p. 116 (1982).

too may be scanned over the specimen. Thus, for nondestructive testing applications, laser generation and detection of ultrasound is an attractive inspection technology in that specimens may be examined remotely, rapidly, and without the need for a coupling medium.

3 RAYLEIGH WAVES

In 1887 Lord Rayleigh proposed the existence of elastic surface waves, suggesting that they "play an important part in earthquakes, and in the collision of elastic solids."[1] Until then only the longitudinal and transverse shear wave modes were theorized as solutions to the elastic media wave equation. In fact, these "Rayleigh" waves, as they came to be called, have been established as having longitudinal and transverse components, but they are categorically recognized as an entirely separate class of propagating waves.

As Rayleigh expected, surface waves are a major component of the waves arising from earthquakes and account for the large disturbances recorded after the initial longitudinal and transverse waves have been received.[2] Accounting for this is the fact that Rayleigh waves propagate with relatively little attenuation when compared to these bulk waves because their existence is essentially limited to a two-dimensional plane. In contrast, longitudinal and transverse bulk waves radiate outward in three dimensions, losing considerable amplitude in much less distance than if they were similarly limited to only two orthogonal directions of propagation. Lesser attenuation makes Rayleigh waves very favorable over bulk waves in numerous ultrasonics applications.

In general, Rayleigh surface waves are modes of propagation of elastic energy along the free surface of an infinite half-space in which the displacement amplitudes of the propagating waves decay in an exponential fashion with depth beneath the surface, so that essentially all of the associated energy is concentrated within a distance of the order of a

1. Lord Rayleigh, *London Math. Soc. Proc.* **17**, 4 (1887).
2. Pollard, p. 71.

wavelength below the surface.[1] This last point is what makes these waves interesting to the study of thin films. Geometrically speaking, thin films are usually characterized as "surfaces", considering their one extreme dimension. Therefore, analyzing surface wave propagation in thin films seems a likely means of material characterization. Generating Rayleigh waves with wavelengths less than the thickness of a given film would allow the measurement of its elastic properties; all of the energy associated with the wave would be coupled to the film material, not the substrate. Though the frequency content of generated Rayleigh waves and the depth to which they penetrate will not be directly addressed by the experiment discussed in this paper, these characteristics constitute the driving factor to applying Rayleigh wave analysis to thin films.

3.1 Other Surface Wave Mode Types

By definition, Rayleigh waves have a longitudinal wave component parallel to the surface and in the direction of propagation, and a transverse component normal to the surface, the resulting particle motion on the surface and at each depth being elliptical, but they are by no means the only type of surface wave. There are a number of others including Love waves (two-dimensional transverse waves involving a transverse component along the surface with particle displacement perpendicular to the direction of propagation), Stoneley waves (waves at the interface between two solids, the wave motion on each side of the interface being of the Rayleigh type), and Lamb waves which propagate in a plate.[2]

For all practical purposes, a sample specimen can be considered a half-space if its thickness is much larger than the wavelength of the surface wave. In this case, Rayleigh wave analysis is valid. Otherwise, the sample will act as a plate, and Lamb wave modes will dominate. In general, only wave modes of the Rayleigh type will be of concern in this thesis, though it will be important to include a rough understanding of generalized Ray-

1. G. W. Farnell, "Properties of Elastic Surface Waves," in *Physical Acoustics*, W. P. Mason and R. N. Thurston, eds. (Academic Press, New York, 1970), Vol. VI, p. 109.
2. Pollard, p. 71.

leigh waves (including Love waves) and pseudosurface waves when introducing anisotropy to the propagating media. A point of interest is that Lamb wave modes can be characterized as a superposition of Rayleigh waves on opposite surfaces of a plate, and vice versa where a Rayleigh wave can be theoretically constructed by superposing the first and second Lamb wave modes.[1]

3.2 Isotropic Solid

On the free surface of an isotropic body, surface waves are referred to as simple Rayleigh waves. The velocity and particle displacements are independent of propagation direction, and the waves are nondispersive.

3.2.1 Velocity calculation

Following the steps taken by Stoneley[2] or Viktorov[3], the velocity of Rayleigh waves propagating on an isotropic solid can be implicitly determined from the familiar equation

$$\left(2-\frac{v_R^2}{v_t^2}\right)^4 = 16\left(1-\frac{v_R^2}{v_l^2}\right)\left(1-\frac{v_R^2}{v_t^2}\right), \tag{3-1}$$

where v_l and v_t are the longitudinal and transverse shear bulk wave velocities, respectively, and v_R is the Rayleigh wave velocity.

Using Timoshenko's notation[4]

$$\frac{v_R}{v_t} = \alpha \tag{3-2}$$

1. B. A. Auld, *Acoustic Fields and Waves in Solids: Volume II* (John Wiley & Sons, New York, 1973), p. 88.
2. R. Stoneley, *Proc. Roy. Soc.* **232A**, 447 (1955).
3. I. A. Viktorov, *Rayleigh and Lamb Waves* (Plenum Press, New York, 1967), Section 1.1.
4. S. Timoshenko and J. N. Goodier, *Theory of Elasticity* (McGraw-Hill Book Company, Inc., New York, 1951), p. 459.

and the relation

$$\frac{v_t}{v_l} = \sqrt{\frac{1-2\nu}{2(1-\nu)}}, \tag{3-3}$$

which states that the ratio of transverse velocity to longitudinal velocity is solely a function of Poisson's ratio, ν, Eq. 3-1 becomes

$$\alpha^6 - 8\alpha^4 + 8\left(3 - \frac{1-2\nu}{1-\nu}\right)\alpha^2 - 16\left[1 - \frac{1-2\nu}{2(1-\nu)}\right] = 0. \tag{3-4}$$

For example, if ν=0.25, the above equation reduces to

$$3\alpha^6 - 24\alpha^4 + 56\alpha^2 - 32 = 0$$

or

$$(\alpha^2 - 4)\,(3\alpha^4 - 12\alpha^2 + 8) = 0$$

which has the three roots

$$\alpha^2 = 4, \qquad \alpha^2 = 2 + \frac{2}{\sqrt{3}}, \qquad \alpha^2 = 2 - \frac{2}{\sqrt{3}}.$$

Of these, only the last root satisfies the condition described by Timoshenko requiring the exponential decay coefficients to be real. Therefore, Rayleigh waves on isotropic solids with Poisson's ratio equal to 0.25 propagate at the velocity

$$v_R = \alpha v_t = 0.9194\sqrt{\frac{G}{\rho}},$$

for transverse shear waves are known to travel at $v_t = \sqrt{G/\rho}$, where G is the shear modulus, and ρ is the density. Since the range of possible values for ν is 0 to 0.5, α correspondingly ranges from 0.8740 to 0.9553, as shown in Figure 3-1.

Implicitly solving Eq. 3-4 for α is rather cumbersome, so a useful explicit approximation to the expression given by Viktorov is often used instead, namely,

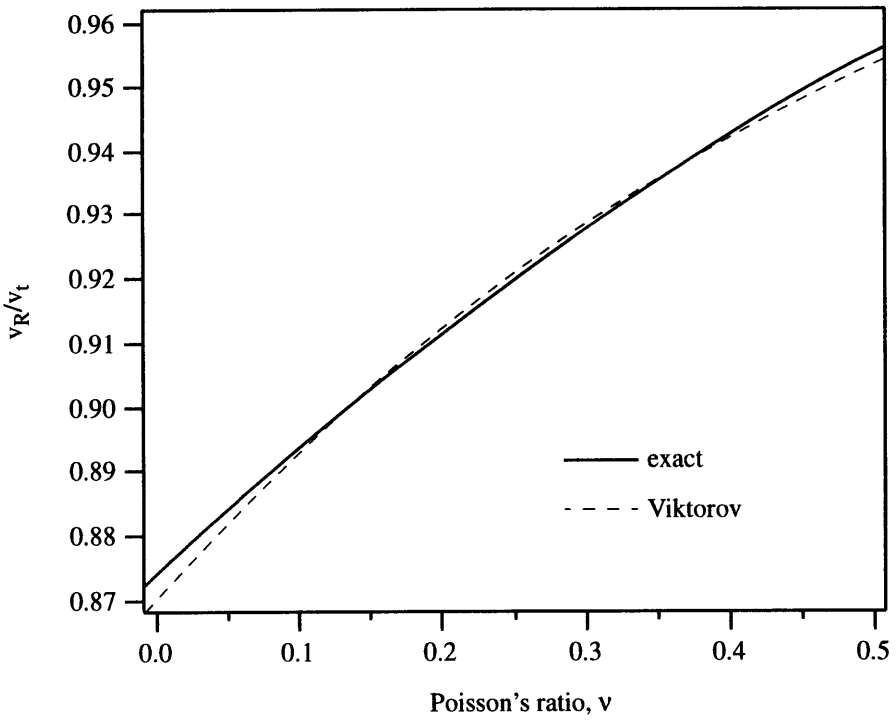

FIG. 3-1. Ratio of isotropic Rayleigh wave velocity, v_R, to bulk shear wave velocity, v_t, as a function of Poisson's ratio, ν. The solid line represents the implicit solution to Eq. 3-4; the broken line is Viktorov's approximation.

$$\frac{v_R}{v_t} = \alpha = \frac{0.87 + 1.12\nu}{1 + \nu}, \tag{3-5}$$

which is accurate to better than 0.5%.[1] This approximation is compared to the exact numbers in Figure 3-1. I prefer to use my own, more accurate approximation

$$\alpha = 0.8654\sqrt{\nu + 1.02} - 0.2228\nu, \tag{3-6}$$

which is accurate to better than 0.2%, simply because every possible reduction of error with respect to velocity calculations improves the accuracy of the laser measurement system described in this thesis.[2]

1. Viktorov, Section 1.1.
2. My approximate solution is not included in Figure 3-1 because it would be difficult to discern it from the exact line.

3.2.2 Particle displacements

For the isotropic case, Rayleigh surface waves are made up of two orthogonal partial waves, namely of the longitudinal and shear types, both having real decay constants into the substrate. The relatively quick decay of these particle motions away from the surface is illustrated in Figure 3-2.[1] The particle displacement field distributions are found by

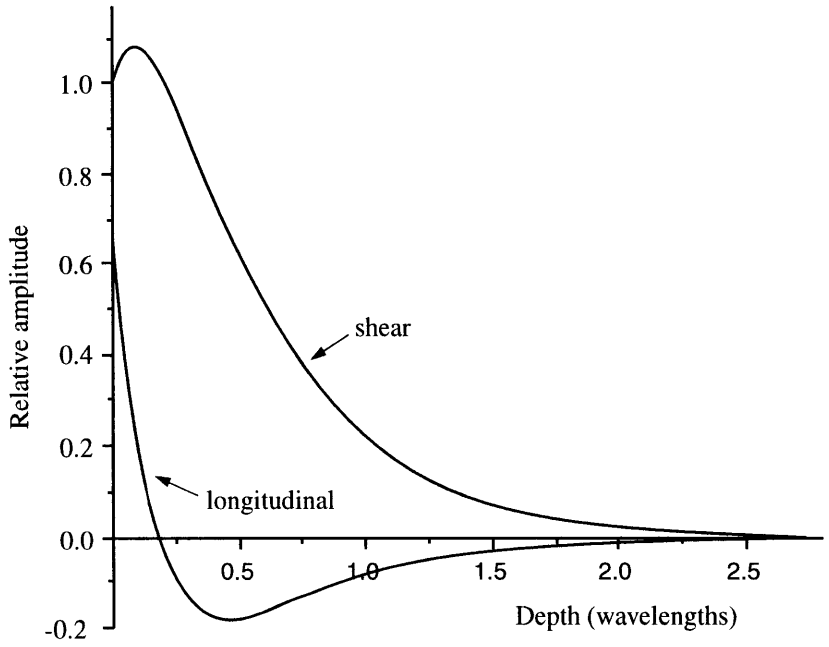

FIG. 3-2. Variation of longitudinal and shear displacements with depth for a typical isotropic material.

combining these two components which are in phase quadrature with each other. The resulting particle displacement at any depth is elliptical, with the plane of the ellipse in the sagittal plane and with the major axis perpendicular to the free surface. Figure 3-3[2] shows that the Rayleigh wave motion is retrograde near the surface and reverses its direc-

1. Farnell, p. 118.
2. Sabine and Cole, p. 104.

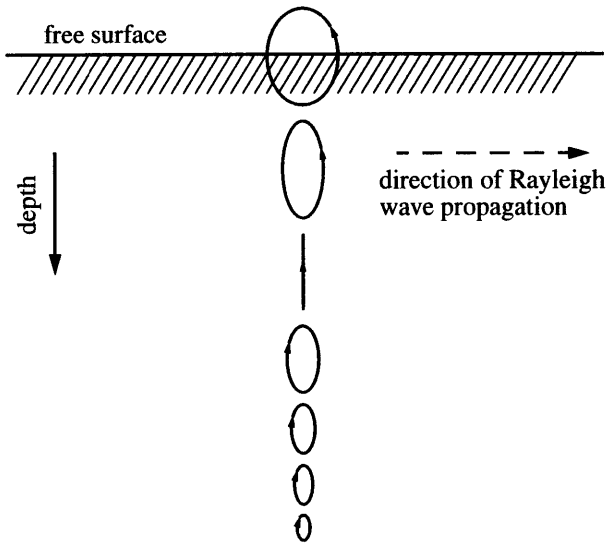

FIG. 3-3. Combined elliptical particle displacements.

tion at depths greater than about 0.18 wavelengths, at which depth the displacement is linearly polarized. This segment supports the statement made earlier that most of the particle motion occurs within a depth of the order of one wavelength which in turn gave rise to the concept that most of the associated energy is concentrated within that depth below the surface.

3.3 Anisotropic Solid

An understanding of surface wave propagation on anisotropic solids is exceedingly more difficult than the previous discussion. For the isotropic problem, it was shown that the Rayleigh surface waves are made up of two partial waves, both having real decay constants into the substrate. On anisotropic substrates these simple solutions occur only for certain special orientations, the decay constants are complex, and the particle motion no longer lies in a plane normal to the surface. Solutions of this kind are sometimes called generalized Rayleigh waves.

Since, a thorough study of surface waves on anisotropic media is given by Farnell[1], only a relatively brief discussion will be included here regarding a few important particulars. Also, because of the careful selection of anisotropic materials to include in the experimentation, further discussion of anisotropic surface waves will be directed toward propagation on cubic crystals.

3.3.1 Velocity calculation

The most obvious change in the character of the surface wave solution on anisotropic materials is the dependence of the velocity on the direction of propagation. Also, on the surface of an anisotropic solid two different transverse modes are possible, in addition to the longitudinal mode. Thus, a more general surface wave is observed whose displacements are three-dimensional. Such a wave may be regarded as a combination of Rayleigh and Love types. A pure Rayleigh wave (or a pure Love wave) can then only be observed when the crystal directions and surface orientation are such that both component waves propagate as pure modes.

Stoneley[2] investigated these conditions in a cubic crystal and showed that, for Rayleigh and Love waves to propagate over a (001) plane, propagation must take place along the [100] or [110] axes. For instance, the velocity equation for a Rayleigh wave propagating over the (001) plane along the [100] direction is

$$c_{11}(\rho v_R^2 - c_{44})\left[\rho v_R^2 - \left\{c_{11} - \frac{c_{12}^2}{c_{11}}\right\}\right]^2 = c_{44}(\rho v_R^2 - c_{11})\,(\rho v_R^2)^2. \qquad (3\text{-}7)$$

Notice that when $c_{12} = c_{11} - 2c_{44}$, the equation reduces to the equation for the isotropic case. Equations of this type for other crystal directions and crystal faces become very cumbersome in the general case, if they can be expressed at all. As Farnell pointed out, "with anisotropic media there are obviously many different combinations of crystal, free

1. Farnell, p. 120–148.
2. Stoneley, p. 447.

surface, and direction of propagation, so that it is impractical to consider all cases; moreover, it does not appear possible to derive omnibus explicit formulas to cover any appreciable range of choices."[1] With this in mind, the experimental velocities for anisotropic crystal samples calculated later in this paper will be compared to the theoretical values predetermined by Farnell and others.

3.3.2 Pseudosurface waves

Another feature of anisotropic surface wave propagation is that of the "leaky" surface wave which has many of the properties of a normal surface wave but has a velocity greater than that of the transverse bulk waves in the corresponding direction. This wave contains a bulk type of partial wave, which radiates or leaks energy into the substrate. At certain critical propagation directions the leaky surface wave becomes totally trapped at the surface and is called a pseudosurface wave[2]; at this point the Rayleigh wave reduces to a pure bulk shear wave which travels along the boundary and itself satisfies the stress-free boundary conditions.

For example, Figure 3-4 applies to the (001) plane of germanium.[3] The shape of the curves is typical of those for the (001) plane of cubic crystals for which the bulk wave with the lowest velocity along [110] has particle displacement in the (001) plane (e.g., Cu, Fe, Si, Al, GaAs, GaSb, InSb, and InAs.) The ordinary surface wave approaches the slow shear wave as the [110] axis is approached and becomes identical with it when the axis is reached. At the same point the pseudosurface wave becomes nonradiating, with two partial wave components and an elliptical particle motion at the surface.

Pseudosurface waves exist on other planar surfaces of cubic crystals, but they will not be of importance in the results. Only on the (100) plane does the pseudo branch become

1. Farnell, p. 120.
2. Auld, p. 131.
3. T. C. Lim and G. W. Farnell, "Character of Pseudo Surface Waves on Anisotropic Crystals," *J. Acous. Soc. Amer.* **45**, 846 (1969).

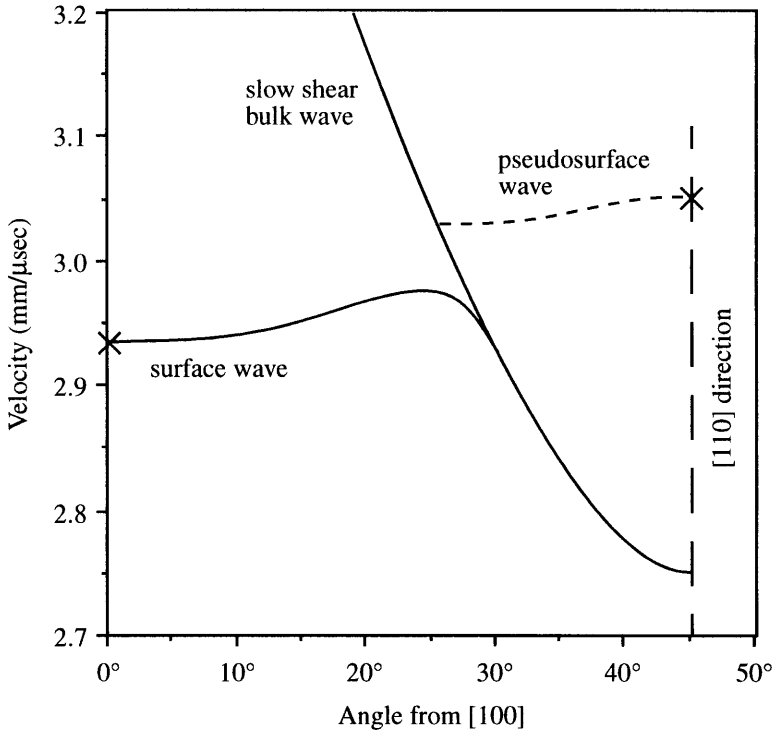

FIG. 3-4. Normal surface and pseudosurface wave propagation in the (001) plane of germanium. ×: Particle displacements lie solely in the sagittal plane.

detectable. Though they are not true surface waves, they are easily observable in experiments involving surface-wave propagation over finite distances. The pseudosurface wave phenomenon will be noticeable, as expected, in the experimental velocity results of the (100)-cut germanium. These waves become detectable over the ordinary surface waves because as the direction of propagation approaches the [110] direction, the normal surface wave particle displacement approaches tangency to the surface, while the pseudosurface wave particle displacement becomes increasingly more normal to the surface. As will become evident later, only the normal particle displacements are detectable by laser detection methods.

3.3.3 Particle displacements

The introduction of imaginary components into the damping factors causes the amplitudes of the corresponding terms in the surface-wave solution to oscillate with depth.[1] Therefore, the amplitudes of the terms will now be of the form of exponentially damped sinusoids rather than the simple exponentials of the isotropic case. Figure 3-5[2] shows the particle displacements given by Farnell for propagation along the [100] axis on the (001) plane of nickel. Just like in the isotropic case, most of the associated energy still lies within one wavelength depth from the surface, and basically all of it exists within two wavelengths.

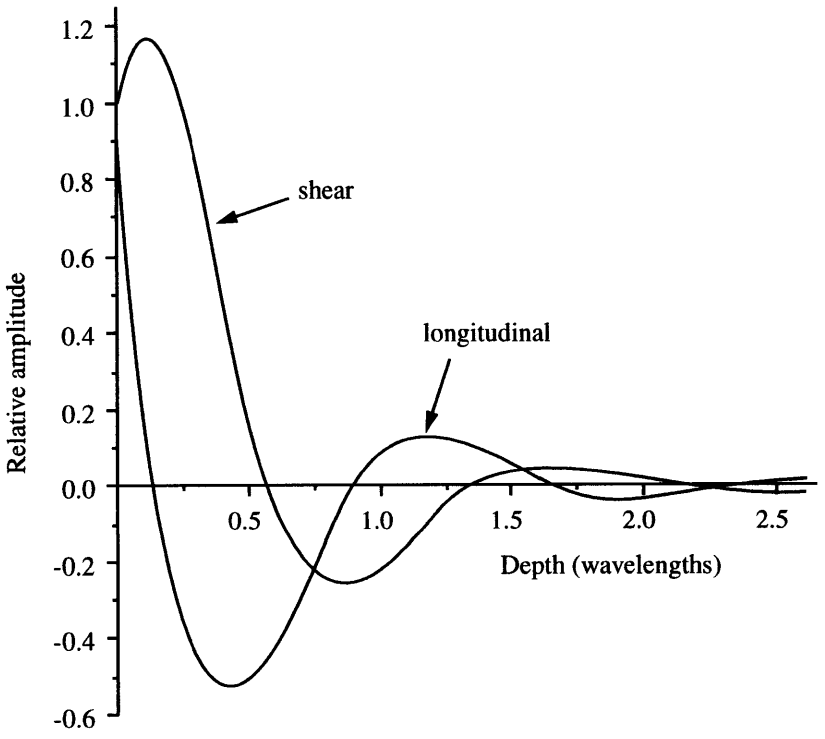

FIG. 3-5. Variation of vertical and longitudinal displacement with depth for propagation along [100] axis on (001) plane of nickel.

1. Farnell, p. 120.
2. Farnell, p. 122.

GENERATION BY PULSED LASERS 4

The mechanisms involved in the laser generation of surface waves can be classified by two general categories: those that involve a change in state of the irradiated medium and those that do not. Under normal circumstances in the absence of any change in state, thermoelastic expansion due to the absorption of laser energy is the dominant mechanism, assuming radiation pressure, electrostriction, and Brilliouin scattering to be negligible effects.[1] But when the optical power density is increased beyond a critical threshold, the material will melt, and then ablation will occur. The acoustic sources generated by these mechanisms differ markedly in terms of the forces produced and their magnitude. A brief discussion of each will be given in the following sections. For a more in-depth study including theoretical and experimental work, see Hutchins.[2]

4.1 Thermoelastic Generation

Consider the irradiation of a clean, solid surface by a Q-switched laser, assuming single pulses of a sufficiently low optical power density, such that the solid is not caused to melt. The optical absorption characteristics of the irradiated medium determine the form of the generated acoustic source. For instance, when the absorption coefficient α is high, as in a metal, the absorbed energy will be localized to within a short distance of the surface, resulting in a source existing over a volume approximated by a thin disk. However, in transmissive solids where absorption is low, the laser beam may penetrate to a consider-

1. Hutchins, p. 23.
2. *Ibid.*

able depth within the medium, and energy will be transferred over a volume approximated by a cylinder with a characteristic length determined by α, the absorption coefficient. For the purposes of this paper, only the first case will be analyzed, but notable differences associated with lower absorption will be cited later in the results.

The degree of absorption in the solid will depend upon the irradiation wavelength, but in general a proportion of the incident laser energy will be absorbed rapidly at the surface and the remainder reflected. This leads to the assumption that significant temperature rises tend to occur only within a small distance from the surface. Hence, the source may be thought of as being localized close to the surface, but just within it. Under such conditions, a simple analysis shows that the stresses formed by thermal expansion will exist primarily in directions parallel to the surface, as shown schematically in Figure 4-1. This process arises because of the presence of a pressure release boundary condition at the object surface, at which normal forces must be zero. The result is a radial expansion source, characterized in general by two orthogonal horizontal force dipoles, only one of which is shown. In fact, in aluminum about 65% of the total elastic energy radiated from a thermoelastically generated point source is carried by the Rayleigh pulse.[1]

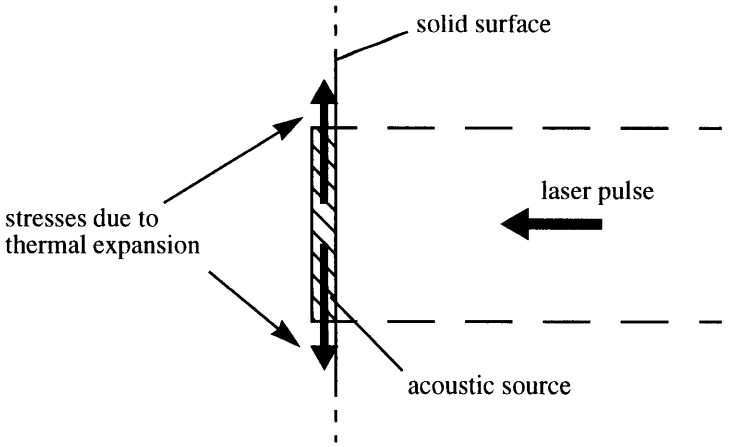

FIG. 4-1. Thermoelastically generated acoustic source.

1. L. R. F. Rose, "On the Energy Radiated by Rayleigh Waves," *Wave Motion* **6**, 359-361 (1984).

The resulting amplitude of the generated wave will be proportional to the incident laser energy, being independent of the area of irradiation.[1] Thus, to a first approximation, it would be expected that small changes in the laser beam diameter (i.e., adjusting the incident power density) will have little effect on thermally generated elastic wave amplitudes, provided directivity factors are not important.

On the other hand, the time duration of the Rayleigh pulse is proportional to the physical diameter of the laser beam (i.e., of the thermoelastic source). This arises because of the variations in the acoustic transit time across the source when the source diameter is changed. For applications where frequency content is important, varying the spot size is a simple means for varying the frequency content of the Rayleigh pulse.

4.2 Ablative Generation

A feature of pulsed lasers is that the optical power density at the region of acoustic generation may be raised by focusing, and, above a certain threshold, a given medium may exhibit a change in state. The material may melt or even ablate, causing an awesome explosion of material ripping away from the surface. Invariably, ablation is accompanied by ionization to form a visible plasma cloud close to the solid surface. Although thermal effects occur at any power density, the magnitude is solely a function of the incident laser energy. As the power density may be increased at constant energy simply by focusing, it is clear that the mechanisms above, which are power density dependent, would tend to dominate the acoustic source at high power densities.

Ablation results in the removal of material from the solid surface and, as just mentioned, is often accompanied by a plasma close to the surface, formed by the removal of electrons from the ablating material. In this case, momentum transfer from ablating material causes forces normal to the surface to exist over the irradiated area[2], as depicted in

1. Hutchins, p. 60.
2. Hutchins, p. 58.

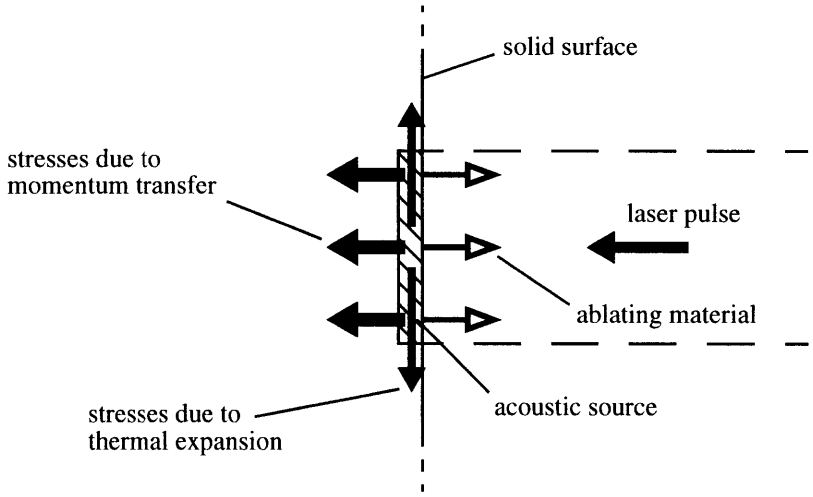

FIG. 4-2. Ablatively generated acoustic source.

Figure 4-2. At high power densities, such forces would predominate, whereas at intermediate power densities above the ablation threshold the source would be expected to contain both normal forces from ablation and forces parallel to the surface from thermoelastic expansion.

In general, ablative generation of surface waves is much more efficient than thermoelastic generation considering the resulting wave amplitude for a given input laser energy. However, the unmistakably destructive nature of ablation precludes its usage in applications geared toward nondestructive testing. Even the slightest melting can corrupt a well-polished surface, so it is important to know the threshold power density. It was noted in the introduction that a nondestructive method would be preferable, but the results of this thesis will show that thermal generation of surface waves is not always easily detectable, namely for those materials which have very low absorption at the excitation laser's wavelength.

4.3 Directivity and the Line Source

In the case of non-destructive testing (NDT), it is important not to cause any surface damage, and, therefore, generation at relatively low laser intensities, where a thermoelastic mechanism operates, is preferable to those intensities where plasma formation on the target surface causes localized damage. However, thermoelastically generated waves are not always detectable without modifications to the surface or to the method of wave generation. There are numerous surface treatments including liquid films and constraining layers which can result in significant changes in the stress distribution, thus increasing the wave generation efficiency.[1] However, surface treatments require altering the specimen and, thus, unfortunately do not fall in line with the concept of NDT.

An alternative technique using a line-focused pulsed laser source, as opposed to the typical point source, generates high amplitude surface wave pulses without surface modification owing to the strong directivity of the generated stress field.[2] For example, an excitation beam focused by a spherically polished lens produces a circular, or point, source thus exciting Rayleigh waves in all directions equally. A line source, however, produced by focusing the beam with a cylindrical lens can be highly directional with well defined maxima in the directions normal to the center of the line axis.

Examples of the angular variation of the amplitude of these two source types are represented as the directivity patterns in Figure 4-3.[3] The angle is defined from the axis perpendicular to the line source. These patterns are representative of those produced for aluminum excited by similar energy laser pulses using a circular 1-mm diameter laser spot and a 4-mm long by 0.1-mm wide laser line, respectively. Theoretically, no wave

1. Hutchins, p. 59.
2. A. M. Aindow, R. J. Dewhurst, and S. B. Palmer, "Laser-Generation of Directional Surface Acoustic Wave Pulses in Metals," *Optics Comm.* **42**, 116 (1982).
3. Aindow *et al.*, p. 118.

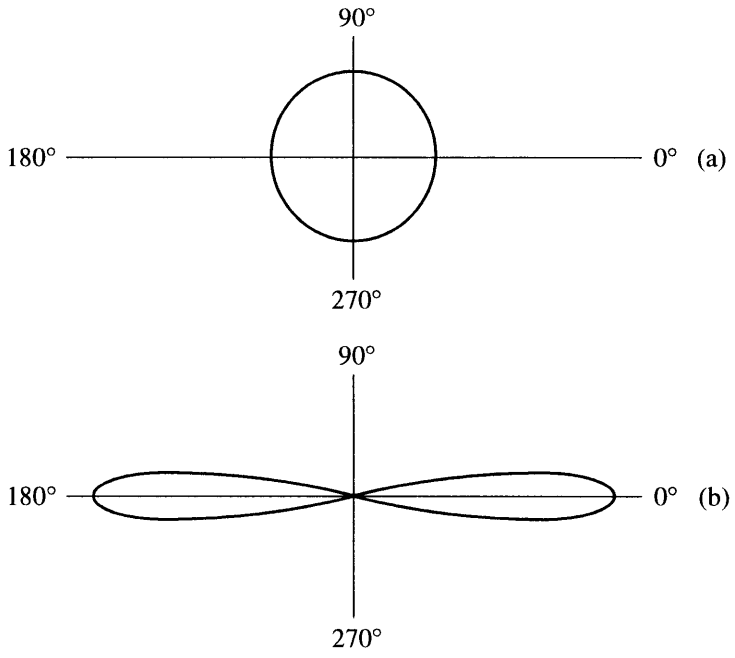

FIG. 4-3. Theoretical directivity patterns on aluminum for (a) a 1-mm diameter point source and (b) a 4-mm by 0.1-mm line source. Distance from the origin represents a unitless amplitude.

energy would propagate in the direction of the line source, but some does due to the finite width of the focused beam.

By concentrating the energy of the Rayleigh wave perpendicular to the line source, a cylindrical lens not only produces directional beams but also enhances the Rayleigh amplitude by a factor of 3 or better. This becomes extremely useful when trying to produce detectable waves without surface damage, for surface waves with amplitudes comparable to those produced by a point source can be excited with a third or less the energy when using a line source.

LASER DETECTION OF RAYLEIGH WAVES 5

A coherent light beam, or laser beam in this case, can be used as a probe to measure the phase and amplitude of acoustic displacements. Various techniques have been employed to detect the effect of the acoustic perturbations on the light beam and to relate the results to the acoustic field parameters. If the cross section of the sampling beam is small compared to the wavelength of the acoustic field as it appears on the sampled surface, the acoustically induced temporal and spatial phase modulation of the reflected beam may be conveniently broken down into three parts:

(a) a periodic phase modulation directly related to the magnitude of the normal surface displacement;

(b) a periodic deflection related to the slope of the surface displacement (tilting of the surface);

(c) a periodic focusing and defocusing related to the curvature of the surface displacement (warping of the surface).

If the sampling beam is many acoustic wavelengths wide, it is more convenient to consider the effect of the acoustic field as equivalent to that of a phase grating, causing multiple diffraction orders to be formed in the reflected beam, thus exhibiting

(d) a temporally and/or spatially periodic phase corrugation which is a replica of the pattern of acoustic displacements.

Each of the effects mentioned lends itself to a particular detection method. The characteristics of the observed surface wave are encoded on the reflected laser beam; the problem is to apply a detection method which decodes that information from the beam. Note that laser-based detection methods assume that the surfaces to be examined are at least partially reflective to the particular laser wavelength.

5.1 Normal Surface Displacement (Interferometry)

When light is reflected from a vibrating surface, the surface displacement gives rise to a corresponding change in optical path length. Thus, for the situation illustrated in Figure 5-1, the total light path traversed by a propagating beam in the absence of any acoustic excitation is simply twice some distance, L, as shown. For a peak surface displacement δ, the optical path is reduced by an amount 2δ. This change in optical path length causes a corresponding change in phase of the optical signal. This change in phase, although contributing to a real and pronounced effect on the form of the optical wave front, cannot be measured directly with conventional instrumentation. In other

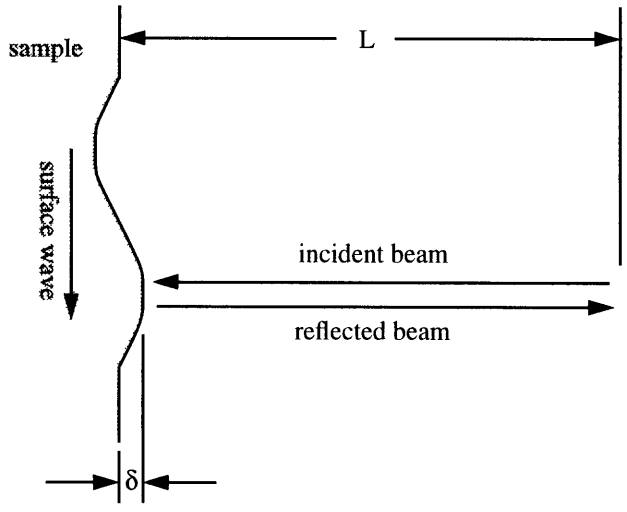

FIG. 5-1. Optical path change, 2δ, imposed by specimen surface displacement, δ.

words, all phase information is lost when intensity or power measurements are made. For this reason, interferometric systems are employed to convert the phase change resulting from surface displacement to intensity variations which can then be measured directly.

The principles of optical interferometry can be understood by considering the Michelson interferometer drawn schematically in Figure 5-2.[1] In this type of interferometer, a beam splitter is used first to separate and then to recombine light from a single optical source. The split beams are directed into separate paths. The reference path is that which proceeds from the beam splitter to a reference mirror and then returns back through the beam splitter to an optical detector. The object path is that path which proceeds from the beam splitter and reflects from the specular surface of the test object before returning to the beam splitter, where it recombines with light from the reference path and is directed onto the same optical detector.

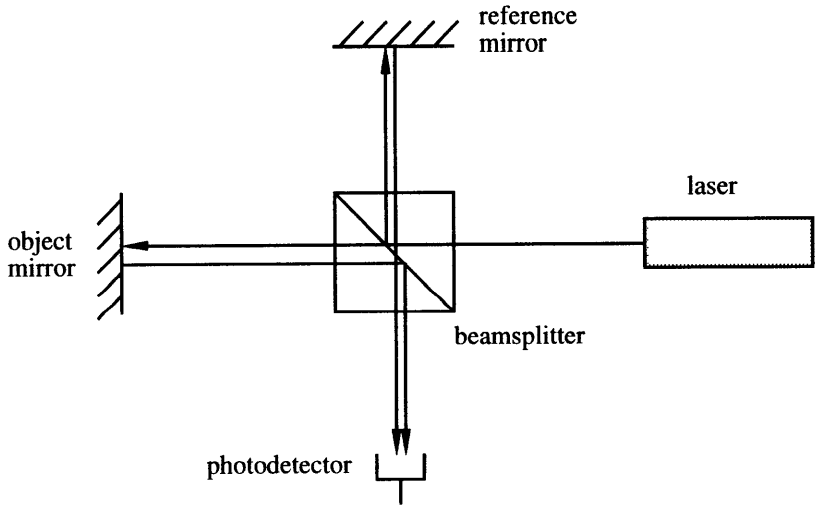

FIG. 5-2. Michelson interferometer.

1. J. W. Wagner, "Optical detection of ultrasound," in *Physical Acoustics* , W. P. Mason and R. N. Thurston, eds. (Academic Press, New York, 1990), Vol. XIX, p. 219.

In practical situations, environmental disturbances such as building vibrations and airborne turbulence generate optical path-length changes that result in a randomly varying interference signal. These path-length changes can have amplitudes of the order of several micrometers (i.e., several fringes), in the 0–1 kHz frequency range. In comparison, transient ultrasonic displacements arising from a laser excitation source are typically of the order of hundreds of picometers to tens of nanometers, representing fractional fringe shifts in the interferometer. Clearly, the interferometer must be stabilized against any low-frequency extraneous mechanical and thermal effects that may alter the optical path-length difference.

Path-length stabilization can be accomplished by implementing an electromechanical feedback loop which uses a piezoelectric element to adjust the position of the reference mirror. For more severe vibration environments, a heterodyne configuration is preferred.

5.2 Tilting of Surface (Beam Deflection/Knife-Edge Technique)

This technique, using an optical setup as depicted in Figure 5-3, uses a knife-edge stop to cause variations in the optical power falling on a detector as a laser beam is deflected by a tilting surface.[1] The figure shows a laser beam focused to a point on an object[2], while a surface disturbance propagates along the object's surface. The angular deviation of the surface at the point from which the light is reflected causes a corresponding change in the propagation angle of the reflected light equal to twice that angle. (Figure 5-4 gives an exaggerated, magnified view of the focused laser beam being deflected by the passing surface wave.[3] Ordinarily, the deflection is too small to be detected by the naked eye.)

1. Wagner, p. 213.
2. The sample's surface does not need to be in the focal plane of lens L_1, but for simplicity and better resolution it will always be assumed to be such.
3. R. L. Whitman and A. Korpel, "Probing of Acoustic Surface Perturbations by Coherent Light," *Applied Optics*. **8**, 1567 (1969).

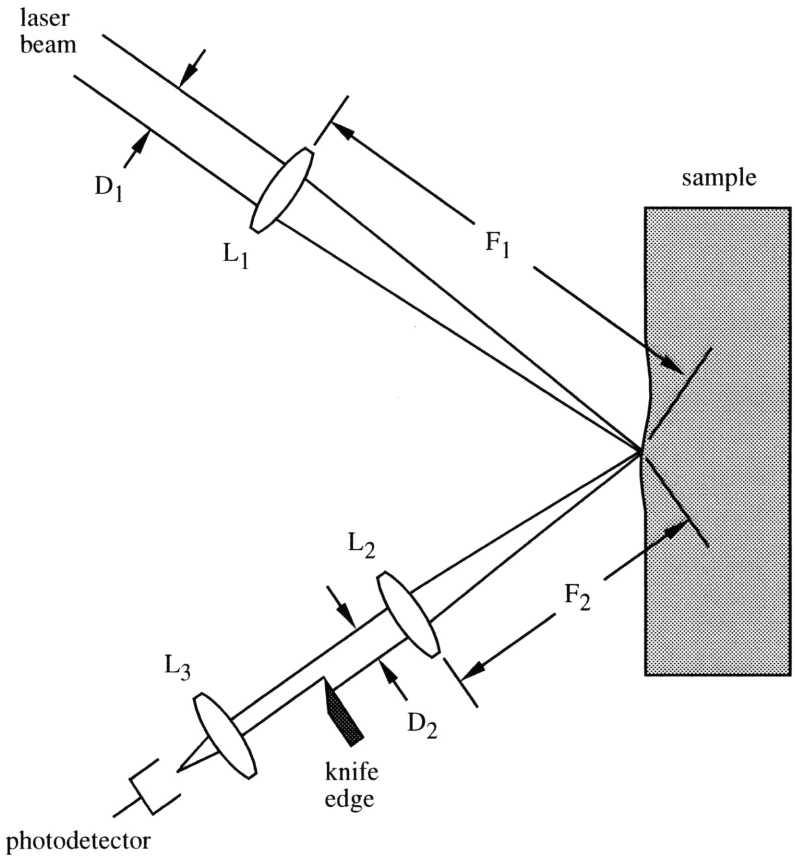

FIG. 5-3. Optical beam deflection (knife-edge) method.

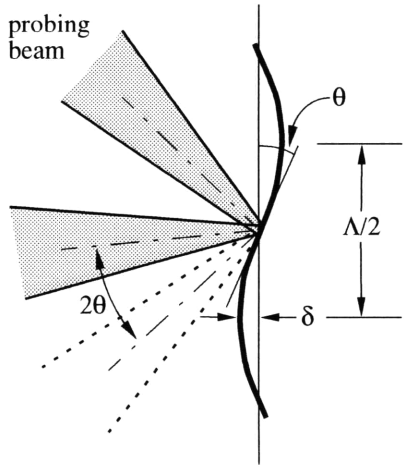

FIG. 5-4. Acoustic surface wave deflecting probing beam.

Lens F_2 is positioned exactly one focal length from the surface so as to recollimate the reflected beam. As the surface tilts, the propagation path of the recollimated beam will deviate from the optical axis which passes through the center of the lens. A knife edge placed behind lens F_2 stops that portion of the recollimated beam which propagates below the optical axis of the lens. Thus the total amount of light which ultimately reaches the optical detector will vary with specimen surface angular tilt. In this manner, photodetection of the resulting laser beam power records the changing slope of a sample's surface due to a surface acoustic perturbation.

5.3 Surface Phase Grating (Diffraction)

The previous two detection methods assumed that the sampling beam was small compared to the wavelength of the acoustic field, but something quite different occurs when the sampling beam is many wavelengths wide. As stated earlier, it is more convenient to consider the effect of a continuous or tone burst acoustic field as equivalent to that of a phase grating, causing multiple diffraction orders to be formed in the reflection beam. The effect is illustrated in Figure 5-5.[1] A broad optical beam normal to the object's surface encounters a region over which there exists a periodic displacement. It is diffracted into several orders so that not all of the light incident upon the surface is directly reflected back along the surface normal. The diffracted orders propagate at angles symmetric about the surface normal according to the grating equation

$$\sin\theta_n = \frac{n\lambda}{\Lambda}. \tag{5-1}$$

The angle of propagation is a function of the acoustic wavelength, Λ, and the optical wavelength, λ.

The diffraction method can be applied in a more general way to detect the arrival of an acoustic surface wave. Consider a laser beam incident on a surface at an angle other than

1. Wagner, p. 217.

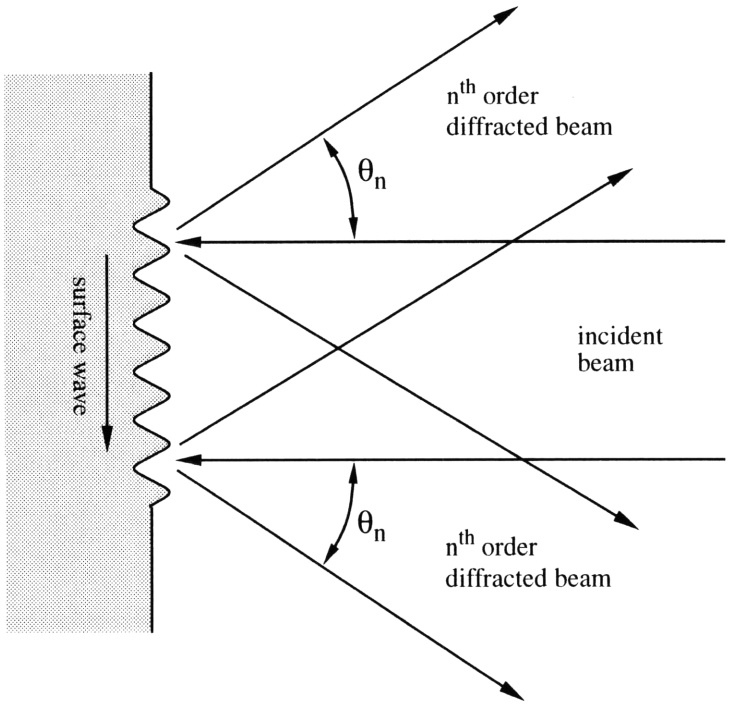

FIG. 5-5. Diffraction of an incident laser beam by a periodic surface wave.

normal as shown in Figure 5-6.[1] A non-normal incident beam introduces a new term to Eq. 5-1. The resulting angles are given by the corrected equation defined by the well-known results of electromagnetic scattering theory[2]:

$$\sin\theta_n = \sin\theta_0 + \frac{n\lambda}{\Lambda}. \tag{5-2}$$

Usually only the first orders are of importance because of their relatively high intensity compared to the higher orders. These two diffracted beams have amplitudes relative to the original reflected beam (main order) given by $2\pi(\delta/\lambda)$ for $\delta \ll \lambda$.[3] In other words, for a

1. A. J. Slobodnik, Jr., "Microwave Frequency Acoustic Surface Wave Propagation Losses in $LiNbO_3$," *Appl. Phys. Lett.* **14**, 95 (1969).
2. P. Beckmann and A. Spizzichino, *The Scattering of Electromagnetic Waves from Rough Surfaces* (The Macmillan Co., New York, 1963).
3. A. Korpel, L. J. Laub, and H. C. Sievering, "Measurement of Acoustic Surface Wave Propagation Characteristics by Reflected Light," *Appl. Phys. Lett.* **10**, 296 (1967).

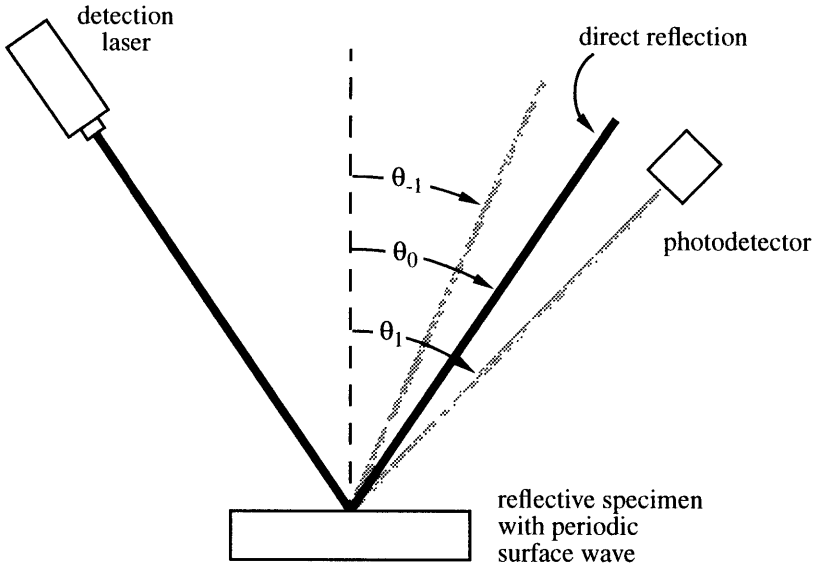

FIG. 5-6. Schematic diagram of diffraction-based experiment for detecting the arrival of acoustic surface waves.

given detection laser wavelength, the amplitudes of the first order beams are proportional to the amplitude of the surface wave. Better sensitivity is achieved by increasing the input wave generation power, and since the diffraction angles are not dependent on the surface wave amplitude, the geometry of the set-up can remain constant for varying wave amplitudes. Only the surface wave wavelength determines the diffraction angle for a given detection laser, so implementing a system based on this method would be relatively simple.

Of course, in most practical situations the detection and measurement of the acoustic signal amplitude by the diffraction grating method requires *a priori* knowledge of the acoustic frequency and its velocity in the material in order to provide optimum detection sensitivity. Otherwise, the acoustic grating spacing and corresponding diffraction angle cannot be known. As is so in this case, since the object of the experiment is to measure the acoustic velocity, the velocity cannot be known beforehand, at least not exactly. However, even limited prior material characterization should provide enough information to

make a reasonable approximation such that fine tuning through a trial and error process should result in precise positioning of the photodetector.

5.4 Deciding Factors for Choosing the Detection Method

Whichever detection method is used, the only information needed from the photodetector signal is the time it takes for the surface wave to travel through a well-defined distance. An absolute time measurement could be made for the time it takes for a wave to travel from the excitation spot to the detection spot, or even better, a differential time measurement could be taken for two different detection spots, the distance and time for which could be more precisely measured. In any case, time is the only relevant information gained from the signal, for the amplitude does not play any part in determining the surface wave velocity.

Usually, the added advantage of interferometry based systems is their simple yet extremely accurate means for extracting the actual wave amplitude, δ, from the electrical signal amplitude. Only the detection laser wavelength and the range of the monitored signal amplitude are needed in the calibration, not the specific laser power or detection sensitivity of the photodetector. But, this comes at a high price, for interferometry requires very expensive, task-specific equipment to path stabilize the system from outside vibrations, which at the onset of this research were decided as needless and avoidable considering the other less expensive, more feasible options. Therefore, for the purposes of this research, interferometry methods will not be further explored.

The great difference between the remaining two detection methods lies in the relative dimension of the detection spot compared to the wavelength of the surface wave. Under normal conditions, the probe size of a focused, diffraction-limited Gaussian beam may be made of the order of $10\,\mu m$ in diameter[1], but that is generally regarded as the extreme

1. A. D. W. McKie, J. W. Wagner, J. B. Spicer, and J. B. Deaton, Jr., "Dual-beam Interferometer for the Accurate Determination of Surface Wave Velocity," *Applied Optics* **30**, 4034 (1991).

practical limit. This greatly puts a restraint on the usage of the knife-edge method, for the probe size must remain a small fraction of the dimension of the surface wave, whether it be the wavelength of a periodic wave or the width of a single pulse, and by no means can it exceed one-half that dimension. For typical materials with velocities in the range of 2000–5000 m/s, this places a wave frequency ceiling of about 100–250 MHz to the detection capabilities of the knife-edge technique. More realistically, the technique should only be used for much larger wavelengths in order to keep tolerable resolution, otherwise the curvature of the wave, as mentioned in the introduction of this chapter, becomes a significant factor.

The diffraction grating method, on the other hand, is limited in its use to higher frequencies, typically requiring there to be at least ten peaks of the periodic surface wave to be spatially captured by the probing laser beam at one time. Stated conversely, the beam width must be at least ten wavelengths in diameter for the zeroth and first order reflections to be clearly defined. Therefore, for a typical helium-neon laser with a 1.5-mm beam diameter, the wave frequency must be greater than 15–35 MHz, but should be more like 100 MHz or higher.

Obviously, the factor that is important here is the type of wave that is generated. A simple, single pulse waveform generated by a single pulse of a Q-switched laser has a pseudo-wavelength on the order of tenths of a millimeter and can be detected by the knife-edge method. The appropriate detection method for a continuous or tone-burst wave, on the other hand, depends on its frequency. The appropriate cut-off region seems to be about 50 MHz. Below that value the knife-edge method should be used, and above it the diffraction grating method should be used.

In the future, the goal will be to detect gigahertz frequency tone-burst waves on thin films such that the wavelength of the generated wave is smaller than the thickness of the film. That will require using the diffraction grating method. However, this paper investigates single pulse waveforms generated by a Q-switched laser source, thus requiring imple-

mentation of a knife-edge optical detection system. The pulsed laser source and knife-edge setup were both simple to implement with existing equipment and were agreed upon as an excellent beginning ground to future work.

6 EXPERIMENTAL SETUP

As described in Chapter 4, the frequency content of the excited wave becomes important when applying surface ultrasonics to thin films. Tone-burst generation would be necessary to provide the concentrated, high-frequency content needed to overcome the dispersive effects of the interface. In this case, however, consisting of research directed initially toward bulk material substrates, it was decided that single laser pulses would be the most appropriate choice. The necessary high-energy laser system would be simple and, fortunately, was readily available at the time. Simplicity being key in the early stages of a many step investigation, the laser detection method was set up in the optical beam deflection configuration utilizing the knife-edge idea, again taking full advantage of presently available resources.

6.1 Excitation

A high-energy, Q-switched neodymium (Nd):YAG pulse laser was used to ablatively and thermoelastically excite surface waves on various bulk material samples. It produced single laser pulses of 45-ns duration with near-Gaussian temporal and spatial energy distribution at a repetition frequency of 10 Hz. Invisible to the naked eye, the infrared YAG laser operated at a wavelength of 1.064 μm.

The energy of the pulses was made variable by passing the beam through a half-wave plate in conjunction with a polarizing beam splitter as depicted in Figure 6-1. The orientation of the half-wave plate determined what fraction of the beam's energy passed through the beam splitter and, consequently, determined what fraction of the available

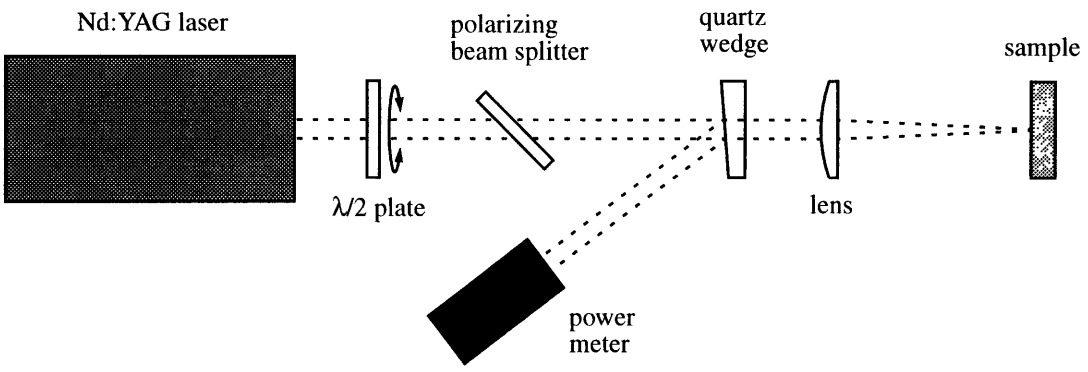

FIG. 6-1. Optical layout of excitation laser.

laser energy irradiated the specimen's surface. The output of the YAG could also be varied by directly changing the delay time between the oscillator and amplifier internal to the laser itself, but the former method provided a remote way of accomplishing the same goal which became extremely useful during periods of intensive data acquisition.

6.1.1 Point source generation

To produce a circular point source on the specimen's surface, the 5-mm beam was focused by a 300-mm focal length spherical lens. A useful approximation for the minimum waist size, w, of a focused beam states that

$$w = \frac{f\lambda}{\pi d}, \tag{6-1}$$

where f is the focal length of the lens, λ is the wavelength, and d is the incoming beam diameter.[1] According to this approximation, the beam waist was about 20 μm at its focused minimum. However, to reduce the energy density on the surface, thus reducing the probability of surface damage, but without reducing the total pulse energy, the samples were moved in closer to the lens at a point where the spot size was about 100 μm. As

1. H. Weichel and L. S. Pedrotti, "A Summary of Useful Laser Equations—an LIA Report," *Electro-Optical Systems Design Magazine*. p. 35 (July, 1976).

stated earlier in Chapter 4, at least for the thermoelastic case, the generated wave amplitude was solely a function of input energy, being independent of the irradiated area. In any case, the larger spot size seemed to result in overall improved signals with less dramatic damage to the surface.

6.1.2 Line source generation

Line source generation, on the other hand, was accomplished by focusing the excitation beam with a 180-mm focal length cylindrical lens. This produced a minimum beam waist of about 12 μm, but again the sample was placed at a distance such that the line width was close to 100 μm. In this way, both the line source and point source had the same dimension in the direction of propagation observed by the detection laser. To a close approximation, by the theory introduced in Chapter 4, the surface wave profile would be similar in both cases having approximately the same pulse width and frequency content.

The line source, being 5 mm long by 0.1 mm wide, thus simulated the point source as if it were stretched by a factor of 50. The width was held constant as a control to observe the effect of the line source directivity. The line source would invariably produce stronger waves than the point source at similar energy levels, subsequently allowing equivalent waves to be produced at much lower energy levels. More importantly, however, with the line source covering a much larger surface area, the energy density irradiating the surface would be 50 times less than the point source with the same total energy. Since the amount of surface damage is governed by the energy density, not the total energy, this would greatly reduce the effects of surface damage, if not overcome them.

6.1.3 Measurement of pulse energy

The additional components in Figure 6-1, consisting of a Scientech volume power meter and a quartz wedge, were included to measure the energy of the YAG's pulses. The partially reflective surface of the quartz wedge allowed 3.5% of the incoming YAG pulse energy to be diverted to the calorimeter disc of the power meter. However, 3.5% of the

energy transmitted through the front surface was also reflected back at a slightly different angle from the back surface of the wedge. Thus, just slightly more than 93% of the beam made it past the wedge. From these numbers, the actual power irradiating the surface was 26.6 times greater than the reading from the power meter, and since the pulses hit the surface at a rate of ten times per second, the individual energy of each pulse was given by 2.66 mJ per mW read off the power meter.

6.2 Detection

The excited Rayleigh surface waves were then detected with a continuous wave helium-neon (He-Ne) laser configured using the principle ideas of the optical beam deflection (knife-edge) method along with a couple added twists to make it more practical for velocity measurement. The 1.5 mW laser operated at 632.8 nm with a beam diameter of about 1.5 mm as it entered the first set of optics.

6.2.1 Sensitivity and resolution

Two important issues regarding any detection method's performance are its sensitivity and resolution. Sensitivity is determined by how responsive the system is, thus governing how small of a wave can be detected, while resolution is determined by the detail with which the wave can be distinguished. Obviously, things would be ideal if these two factors were independent of each other and could each be bettered without sacrificing part of the other. But, as always, there is a trade-off. Unfortunately, it will be shown that they are inversely determined by the same geometric variable, therefore disallowing them to be optimized independently of one another.

The responsiveness of the knife-edge technique is defined by the variation in the optical power reaching the detector as a function of the acoustic disturbance. The following analysis by Wagner[1] shows how the signal power is determined by the geometric place-

1. Wagner, p. 214-215.

ment of the optical elements in addition to the obvious parameters including the total incident power and wave amplitude. In this case where a small gas laser was used as the light source, the local electric field amplitude, a(x,y), at the knife edge varies over the cross-section of the beam with the Gaussian dependence

$$a(x, y) = \frac{a}{d}\sqrt{\frac{2}{\pi}}e^{-\frac{(x^2+y^2)}{d^2}} . \tag{6-2}$$

In Eq. 6-2, d is defined as the radius at which the field drops to 1/e times its central (maximum) value. The integration

$$I_{total} = \int_{-\infty}^{\infty}\int_{-\infty}^{\infty} |a(x, y)|^2 dxdy = a^2 \tag{6-3}$$

verifies that this electric field amplitude variation gives the correct total intensity.

With the beam centered on the knife edge as show in Figure 6-2, a small deviation of the laser beam by an amount Δy will give a corresponding change in optical intensity reaching the detector. For very small angular deviations ($\Delta y \ll d$), the intensity varies in direct proportion with the beam deviation, Δy, as follows:

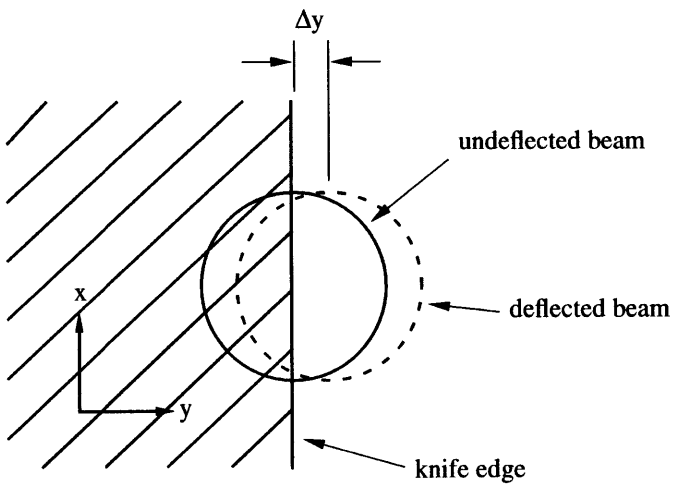

FIG. 6-2. Projection of the optical beam onto a knife-edge produces a change in total transmitted optical intensity for a beam deflection, Δy.

$$I_{sig} = \Delta y \int_{-\infty}^{\infty} |a(x, 0)|^2 dx$$

$$= \sqrt{\frac{2}{\pi}} \cdot a^2 \cdot \frac{\Delta y}{d}. \tag{6-4}$$

Since the irradiance and total incident power have the same functional dependence as the intensity, the total incident power P_i, the signal power reaching the detector, P_{sig}, may be expressed as

$$P_{sig} = \sqrt{\frac{2}{\pi}} \cdot P_i \cdot \frac{\Delta y}{d}. \tag{6-5}$$

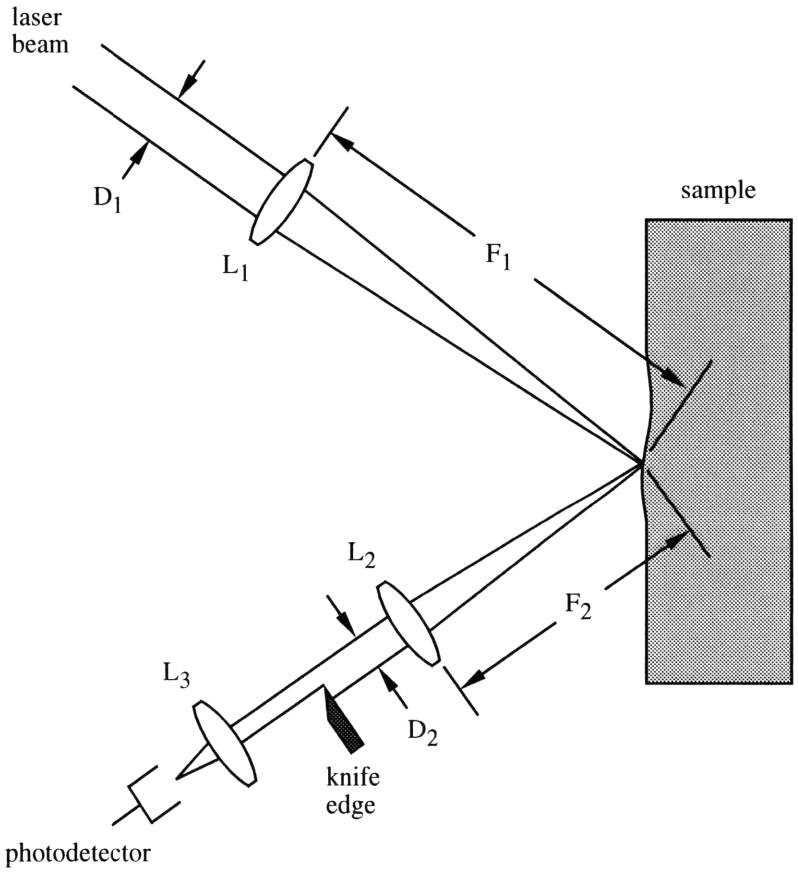

FIG. 6-3. Optical beam deflection (knife-edge) method.

Consider again Figure 5-3 of Chapter 5, now redepicted in Figure 6-3. For a surface angular deviation, θ, the corresponding displacement of the recollimated beam axis will be

$$\Delta y = F_2 \tan 2\theta, \tag{6-6}$$

which is approximately $2\theta F_2$. Also, since the knife edge is the location of observation, d is now the same as $D_2/2$, so Eq. 6-5 becomes

$$P_{sig} = \sqrt{\frac{2}{\pi}} P_i 4\theta \frac{F_2}{D_2} \ . \tag{6-7}$$

One can see that the optical power variation at the detector is proportional to the amplitude of the acoustic surface displacement and the total incident power, as expected. Obviously, the more significant the event, the greater the response will be in the signal. More characteristic to this particular detection method, however, is its dependency on the geometry of the setup, which is suggested by the linear dependence on the ratio F_2/D_2. Two important factors are involved in that ratio: the lever arm and spot size of the reflected beam. They work together to determine how large of a change in the beam intensity passing the knife edge will be produced by a given surface tilt. The translation of the beam cross-section across the knife edge is determined by the lever arm of the reflected beam, while the beam cross-section determines the fractional change in the intercepted intensity for a given displacement across the knife edge. In other words, greater response or sensitivity can be achieved by increasing F_2, the focal length of the output beam, and/or decreasing D_2, the output beam diameter.

More realistically, a better, more direct approach is to establish the parameters of the input beam rather than of the output beam. Using geometric considerations, the ratio F_2/D_2 in Eq. 6-7 can be replaced by F_1/D_1. Therefore, the sensitivity is bettered by increasing the ratio F_1/D_1.

The resolution of the system is defined by the relative size of the probing laser spot with respect to the dimension of the surface wave. Section 5.4 discussed how the probe size must be a small fraction of the surface wave dimension for the knife-edge method to yield acceptable results. Improved, more accurate detail is achieved by decreasing the spot size, thus bettering the resolution. Quantitatively, the resolution of a knife-edge setup for a specific excited wave is given by the probe size as defined in Eq. 6-1. For a beam diameter D_1 and lens with focal length F_1 the equation becomes

$$\text{probe size} = \frac{\lambda}{\pi} \cdot \frac{F_1}{D_1} \tag{6-8}$$

thus showing the dependence of the resolution on the ratio F_1/D_1. However, to increase the resolution, it is important to reduce the probe size which requires lessening the ratio F_1/D_1.

Neither the sensitivity nor the resolution of the knife-edge system can be improved without degrading the other. Therefore, it becomes important to optimize the system with respect to these two concerns in view of the expected size and dimension of the detected surface waves.

6.2.2 Optical layout

In consideration of the previous argument, a spherical lens with a focal length of 300 mm was used for lens L_1, and the incoming beam diameter D_1 was kept at the unaltered He-Ne beam width of 1.5 mm. No quantitative judgement was made regarding the choice of focal length; however, a qualitative trial and error process investigating focal lengths between 100 and 500 mm showed that the 300-mm lens resulted in clearly distinguishable detail and seemingly reasonable sensitivity. The shorter length lenses resulted in greatly reduced signal amplitudes, while the others tended to average out the varying surface information again resulting in reduced signal amplitudes.

Normally the reflected beam would then be recollimated before passing the knife edge, but really lens L_2 is only included to more easily understand the equations defining the sensitivity of the system. It can be removed without changing any of the previous analysis; lenses L_2 and L_3 need only be combined into one stronger lens in the place of L_3. Either way is correct, but removing L_2 saved space on a tightly cramped work space.

Thus, the reflected beam passed directly by the knife edge through a tightly focusing 30-mm lens and into the 400-μm aperture of a Nu Focus model 1601 DC–1 GHz low noise silicon photoreceiver. For optimal results it was important that the reflected beam be intercepted by the knife edge such that 50% was stopped, and 50% was allowed to pass. This produced the greatest variational intensity in the unintercepted beam for a given surface disturbance.

6.2.3 Method for accurate distance measurement

Half of accurately determining the Raleigh wave velocity lies in accurately measuring the distance between two known points along the path of the propagating wave. Of course, a very crude calculation can be made by measuring the distance between the excitation spot and detection spot, but the error involved is too large. Even magnifying the area does not yield much improvement, for the main difficulty lies in measuring an accurate distance between two very fuzzy, ill-defined spots of light.

A much better method is to impose an extremely accurate known distance between two points, rather than to attempt to accurately measure the distance between them. Imposing the distance allows for much greater precision than measuring an arbitrary distance, for the error is determined by the smallest discernible resolution of the micropositioning device used to impose the distance which for some micropositioners is as small as a micron.

McKie, *et al.,* investigated a dual-probe interferometer for making high-accuracy absolute surface wave velocity measurements by way of a precision differential measurement of

the distance between the two probes.[1] A single He-Ne beam was split into two separate probing beams by two polarizing beam splitters and then recombined into a single beam yielding one signal encoded with information from the two detection spots. The relative distance between the probes was carefully controlled by moving the beam-splitter cubes perpendicular to the sample's surface with a micrometer translation stage. Thus, the separation of the two He-Ne probes was adjustable with a spatial resolution of 2 μm.

The dual-beam approach functioned well with the interferometry-based detection method, but with the deflecting beam of the knife-edge technique, a different approach needed to be taken. It was decided that an easily moveable, single probing beam could accomplish the same precision as McKie's dual-probe configuration by comparing two successive signals instead of gathering all the information from just the one. Of course, two signals take twice as long to gather, but a time savings of a matter of seconds is not usually worth the much larger expense of the interferometry setup.

Signals from two different detection spots could be gathered using the brute force method of redirecting the beam to a different location, but realigning all the optics is no pleasant task, not to mention that the distance between the two spots would not be imposed but, rather, would have to be measured. So, a practical method of moving the detection beam across the surface would require implementing a micropositioning device in such a fashion that the optics could be left alone, i.e. would not need realigning before each test.

After investigating a few novel ideas, a very simple method using a micropositioning translation stage demonstrated promising merit. It stemmed from the obvious idea that placing all of the detection system's components on a single translation platform would quickly solve the problem at hand. However, because of the spread-out nature of the knife-edge technique's layout, that would hardly be practical. A translation stage that size is by far not readily available, if it exists at all. But, with the proper modifications, only a

1. McKie *et al.*, p. 4035.

few necessary components needed to be placed on a translation stage to give the same result.

The final detection setup with the micropositioning translation stage in place is shown in Figure 6-4. Only the focusing lens, L_1, and the knife edge were placed on the stage along with a mirror which directed the He-Ne beam along the correct path. The beam was brought into the stage area parallel to the stage's direction of movement, allowing the stage to move without affecting the beam's path in the stage's spatial frame of reference. In this manner, the beam always travelled through the center of the first lens and by the edge of the knife blade. The translation of the stage directly determined the motion of the detection spot along the sample's surface. In effect, the precision of the imposed distance of one spot relative to another was better than one ten-thousandth of an inch, or 2.5 μm, the smallest ruled increment on the vernier micrometer used to position the translation stage. Note that the translation of the stage and detection spot was in the horizontal plane, so the excitation spot needed to be positioned at the same height on the sample's surface, horizontally in-line with the detection spot's travel.

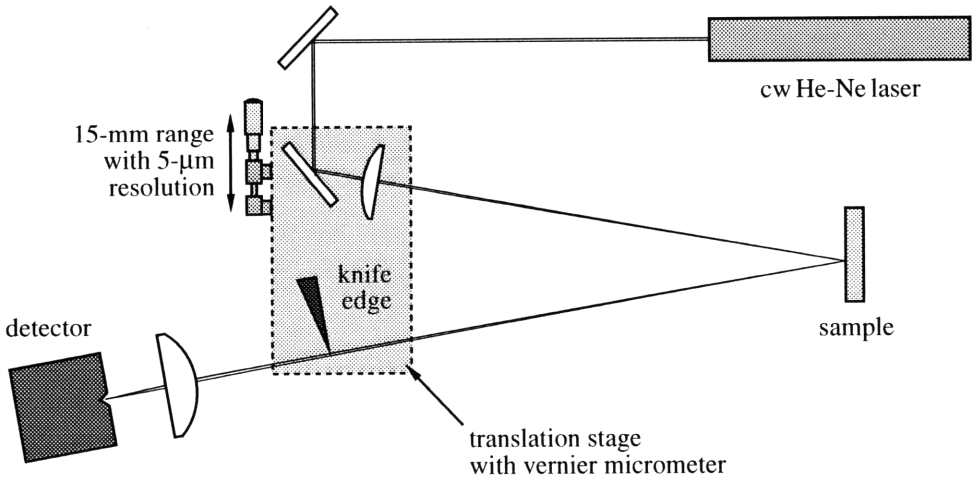

FIG. 6-4. Detection system configuration utilizing translation stage for accurate distance measurement.

The remaining consideration involved getting the reflected beam focused into the small aperture of the photodiode for a wide range of translation. The beam as it passed by the knife edge and entered the last lens was approximately collimated, so to a close approximation the lens would have theoretically focused it to a fixed point in space one focal length away along the center axis of the lens as long as the incoming beam remained parallel to that axis. However, the slight divergence of the reflected beam and the strong spherical aberration of the tightly focusing 30-mm lens limited the validity of that argument. With a few small adjustments to the placement of the lens and photodiode, a total range of more than 15 mm was achieved with full sensitivity throughout the range. Beyond the range, though, the focused beam no longer fully entered the photodiode's aperture, but considering that the test samples were only 2.5 cm in diameter, that range was more than enough.

For very well-polished surfaces, the knife edge nominally intercepted 50% of the reflected beam throughout the range without any adjustment to the position of the knife edge. However, the microscopic unevenness of the surfaces of a few samples, especially the aluminum ones, caused the beam to deflect from the intended axis as the spot was moved across the surface. This minimal deviation did not interfere with the range of acceptance into the aperture, but it did require slight repositioning of the knife edge for each new detection spot. With the knife blade held by an adjustable mount, a simple turn of a screw taking a few seconds was all that was needed to bring the detection system back to optimum sensitivity.

6.3 Signal Processing

The remaining system consisted of the equipment necessary to view and digitally record the signal produced by the photodiode. The signal was amplified with a high-gain amplifier and displayed through a Tektronix 7094 oscilloscope equipped with a digital camera which enabled the trace image to be enlarged onto a television screen. Utilizing the television facilitated the real-time viewing of the signal important to making repetitive

adjustments before and between tests. The images captured by the camera were also input to a PC equipped with the camera's data acquisition software. These snapshots of the oscilloscope traces could then be digitally recorded to disk and analyzed at a later convenience.

6.4 The Complete System

Together the three systems combined to form the complete Rayleigh surface wave velocity measurement system shown in Figure 6-5. Figure 6-6 shows the relative locations of the line source and detection spot on the surface of a sample supported in a Newport optical mount. The line source was positioned about 5mm from one edge allowing plenty of

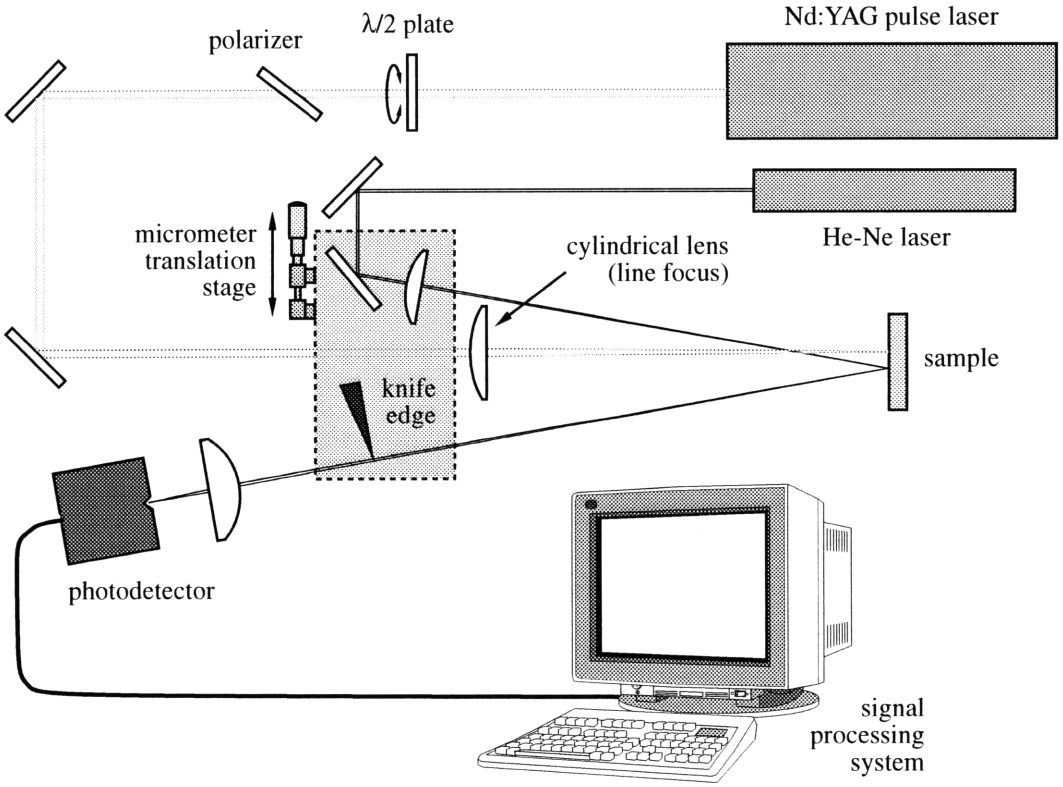

FIG. 6-5. Complete experimental setup including the excitation, detection, and signal processing systems.

travel for the detection spot while keeping any reflected waves from interfering with the first arrival. With a range of 15 mm, the He-Ne laser was positioned such that the detection spot was typically adjustable from ~3 to ~18 mm away from the excitation source. In the figure, the detection spot appears twice to illustrate the available 15-mm range.

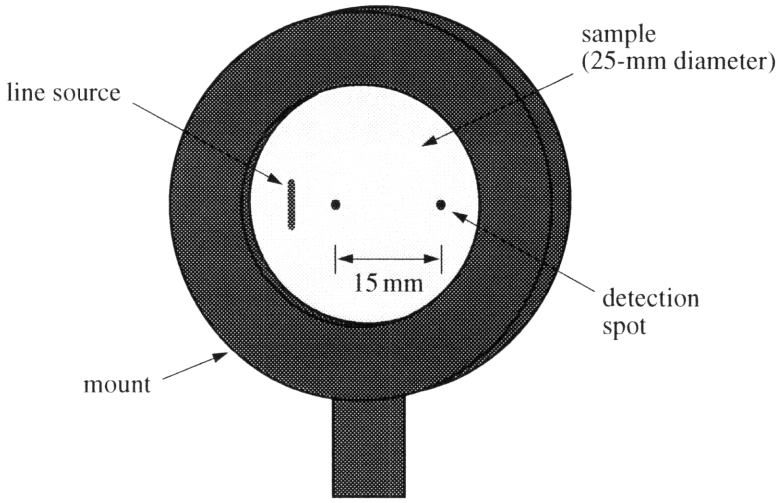

FIG. 6-6. Front view of a mounted sample showing the relative locations of the line source and detection spot. The excitation laser is focused to a point approximately 5 mm from one edge to keep reflected waves from interfering with the first arrival.

7 PROCEDURE

7.1 Oscilloscope Trace

The oscilloscope was externally triggered by the same electric signal which triggered the Q-switching of the Nd:YAG laser. This resulted in traces similar to the one shown in Figure 7-1. The quick, steep pulse on the left-hand side is produced by scattered radiation from the excitation laser. Although the photodiode is relatively insensitive to the infrared wavelength of the YAG, the intensity of the laser light scattered at the excitation source toward the photodiode is great enough to produce the spike at the left. This characteristic of the trace represents time zero when the target is hit, with negligible error due to the travel time of light, and gives an excellent fixed point from which to make time measurements.

This particular trace is representative of an initial test run on gallium arsenide (GaAs) oriented in an arbitrary crystal direction. The surface was ablated using a high-energy point source, exciting not only radially propagating Rayleigh surface waves, but also a spherically propagating shock wave caused by the intense explosion of ablated material. This phenomena, known as a blast wave[1], produces the large excursion of the signal at the right of the figure. The wave is generated at the gas-solid interface and travels through the air, not in the material. The pressure gradients that accompany the blast wave cause gradients in the refractive index of the air around it, thus deflecting the detection beam and falsely mimicking a surface wave. Its velocity and arrival time depend on the energy

1. T. Zyung, H. Kim, J. C. Postlewaite, and D. D. Dlott, "Ultrafast imaging of 0.532-mm laser ablation of polymers: Time evolution of surface damage and blast wave generation," *J. Appl. Phys.* **65**, 4557 (1989).

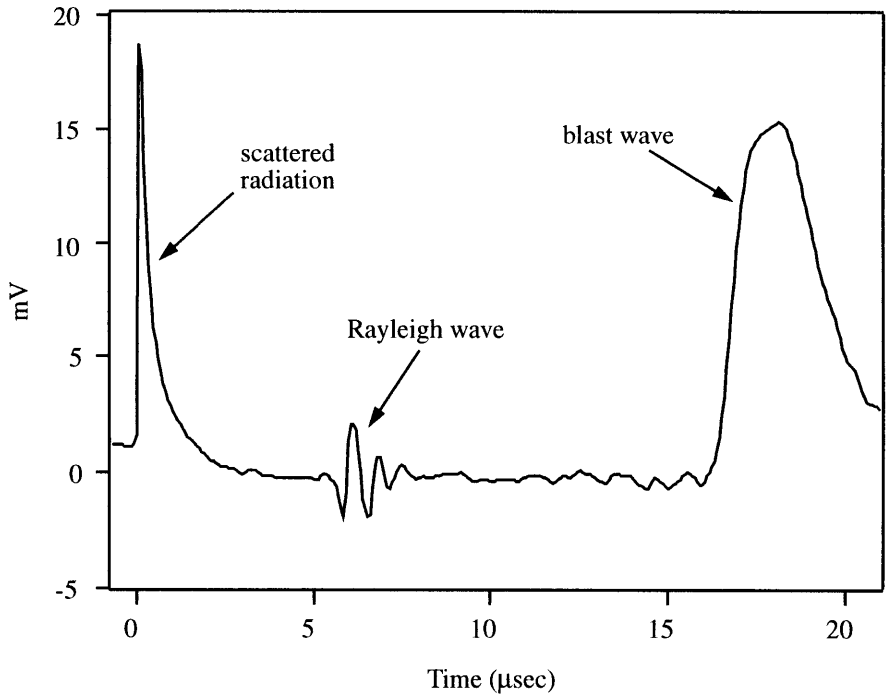

FIG. 7-1. Typical oscilloscope trace.

deposited by the laser, distinguishing it from the Rayleigh surface waves which have an energy-independent velocity. Blast waves are not generated when the surface is irradiated below the ablation regime.

The Rayleigh wave signal is small in comparison but still clearly visible, it's trace representing the time derivative of the sloping surface. Figure 7-1 shows the Rayleigh wave arriving considerably before the blast wave, but this is not always the case. Initially the blast wave travels at speeds an order of magnitude faster than the surface wave, but quickly slows down due to air resistance.[1] The surface wave typically catches up within a millimeter or two, thus giving an unhindered view of the Rayleigh wave within the detectable range of 3–18 mm from the source. Otherwise, the blast wave would interfere with the optical detection of the surface waves.

1. Zyung *et al.*, p. 4558.

As a side note, a special feature of the camera's software package was the ability to quickly capture and average numerous oscilloscope traces. Taking an average over 10-20 signals resulted in much smoother, cleaner traces by greatly curtailing the effects of random noise and unexpected anomalies. In effect, averaging many signals increased the signal-to-noise ratio thus bettering the minimum detectable signal.

7.2 Velocity Calculation

Chapter 5 explained why a single observation with only one detection probe does not present adequate information to make an accurate velocity calculation. Not only is there much room for error when measuring the distance between the excitation and detection spots, but an oscilloscope trace is too vague to make an accurate absolute time measurement between the time of excitation to the time of detection. The trace in Figure 7-1 helps to make this point clear. Even with the information gathered from a single trace, it remains unclear exactly when the surface wave is generated and when it first reaches the detection probe. Obviously, as seen by the finite temporal width of the Rayleigh wave signal, the wave is not generated all at once, but rather is excited gradually by a very complicated time-dependent mechanism.

Also, the excitation source does not exist solely at the extreme surface of the solid, but rather penetrates to within a certain depth of the surface. The generated transients take time to reach the surface before propagating along it as steady surface waves. In other words, the event occurring at generation is too complicated to define any one time as time zero. Therefore, the scattered radiation spike in the oscilloscope trace, which does remain relatively constant throughout any given set of tests, can only be used as a reference time, not as the absolute time of surface wave generation.

With the above understanding, accurate time measurements were made by observing the propagation of one characteristic feature of the wave signal, usually the center of the largest peak, relative to the scattered radiation spike. For example, an overlay of a series of

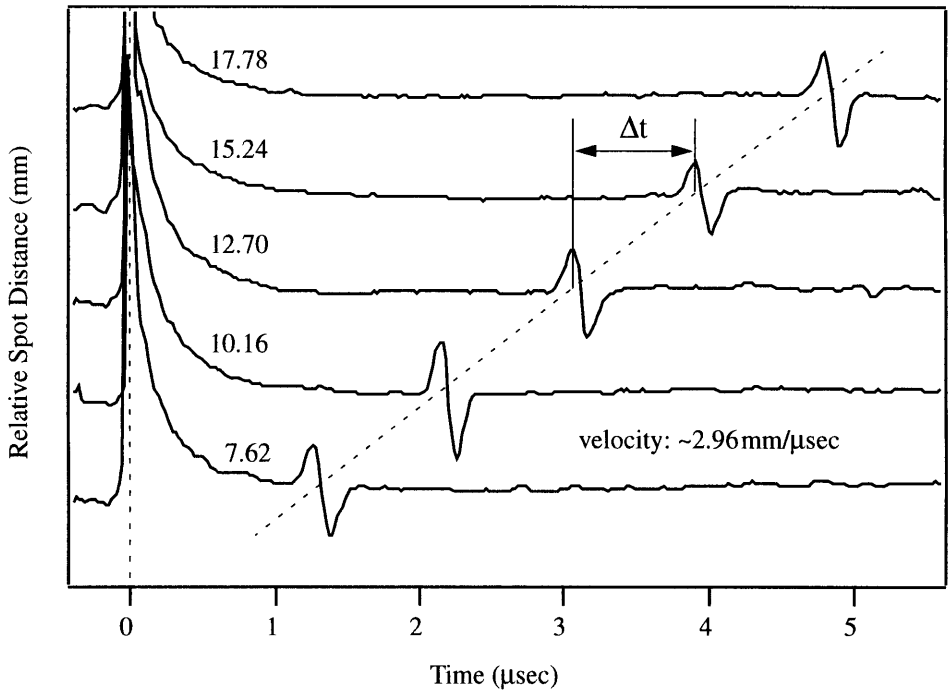

FIG. 7-2. Time history plot of surface waves on an unknown aluminum alloy showing time traces taken at five successive detection spot locations. The plots are spaced according to their relative distance to an arbitrary reference point on the samples surface.

traces is given in Figure 7-2 to show the time history of the progression of a typical surface wave on an unknown aluminum alloy specimen. The traces are vertically spaced according to their relative distance to an arbitrary reference point on the sample's surface typically determined by where the zero mark on the micrometer placed the detection probe. The incremental distance was kept constant to show the linear progression of the wave pulse, as indicated by the line going through the center of each of the first peaks.

The information from a complete set of traces was then plotted, and a line was curve fit to the data using a least-squares algorithm. Figure 7-3 illustrates an example of this plot for the same aluminum sample. Note that since the distance and time measurements were made relative to arbitrary reference points, not the point of generation, the line does not intersect the origin. Nevertheless, the velocity is still determined by the slope of the line.

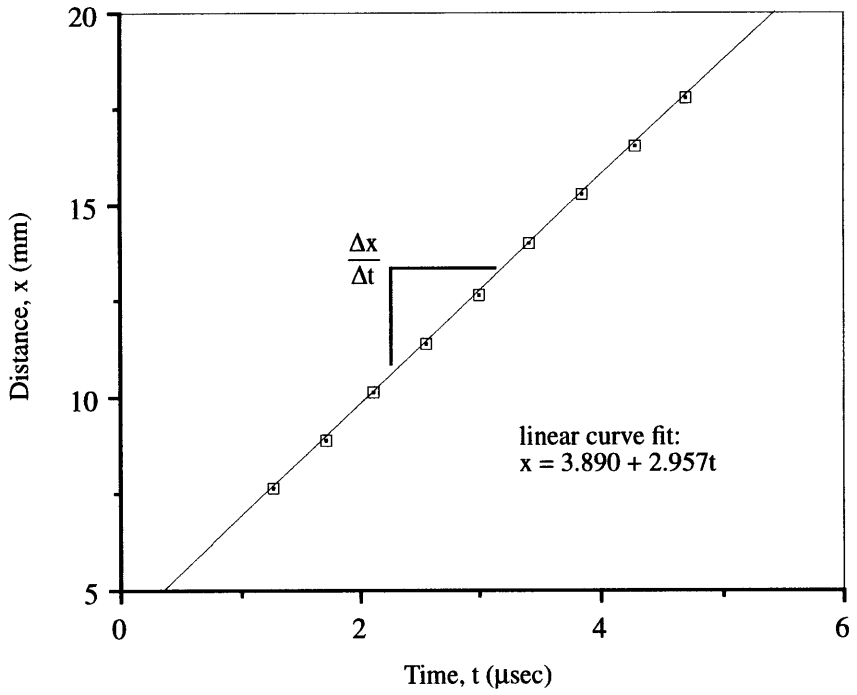

FIG. 7-3. Distance vs. time plot for an unknown aluminum alloy. A linear curve fit shows the Rayleigh wave speed, determined by the slope of the line, $\Delta x/\Delta t$, to be 2.96mm/μsec.

Here the velocity of Rayleigh waves propagating on the surface of the aluminum sample was calculated at 2.96mm/μsec.

7.3 Error Analysis

The estimated error in the velocity calculation is determined by two factors: distance measurement error and time measurement error.

7.3.1 Distance measurement error

As described earlier, the translation stage incorporated a vernier micrometer with a resolution of 0.1mil, or 2.54μm, limiting the accuracy of the imposed relative position of the detection probe to within ±2.54μm. But, since the distance measurements were determined by the difference of two detection spots' positions, they were subject to the error of

both spots' positions. Thus, the accuracy of a distance measurement was limited to $\pm 5\,\mu m$. Spatial resolution could easily be improved by employing a more precise micropositioning device, say one accurate to $\pm 1\,\mu m$, but it will be shown that distance measurement errors were overshadowed by the limited temporal resolution of the captured signal traces.

7.3.2 Time measurement error

Determining the error involved in making time measurements is a little less prescribed than the previous explanation. To aid in the argument, Figure 7-4 presents again a typical signal trace that has been captured and stored by the computer. Although the analog oscilloscope produces a smooth, unbroken trace, the computer software stores the information as 512 discrete data points. Therefore, without further insight, time measurements would be subject to error equivalent to ± 1 point.

The scattered radiation spike and the first peak of the Rayleigh pulse from the complete trace in Figure 7-4(a) have been magnified below it to illustrate this discretization. Notice how few points actually establish the outline of these two distinctive features. Here, the data points are approximately $0.02\,\mu sec$ apart. Accordingly, when using only these data points, the observed times at which the spike and the Rayleigh pulse peak are subject to $\pm 0.02\,\mu sec$ of error, meaning that the time passed between the events is accurate to only $\pm 0.04\,\mu sec$, and the error involved in comparing the travel time of two different Rayleigh pulses is then twice that.

Fortunately, the shapes of the scattered radiation spike and the Rayleigh pulse show that time can be observed with considerably better accuracy than is directly admitted by the discrete data points, i.e. through reasonable interpolation. For example, consider the magnified Rayleigh pulse in Figure 7-4(c). The previous argument states that the pulse's maximum point occurs between 3.04 and $3.08\,\mu sec$, but, obviously, it lies without doubt within a much smaller window. More reasonably, yet still allowing for liberal error, the peak should be observed at $3.06\,\mu sec$ give or take $0.01\,\mu sec$, not $0.02\,\mu sec$, and a time

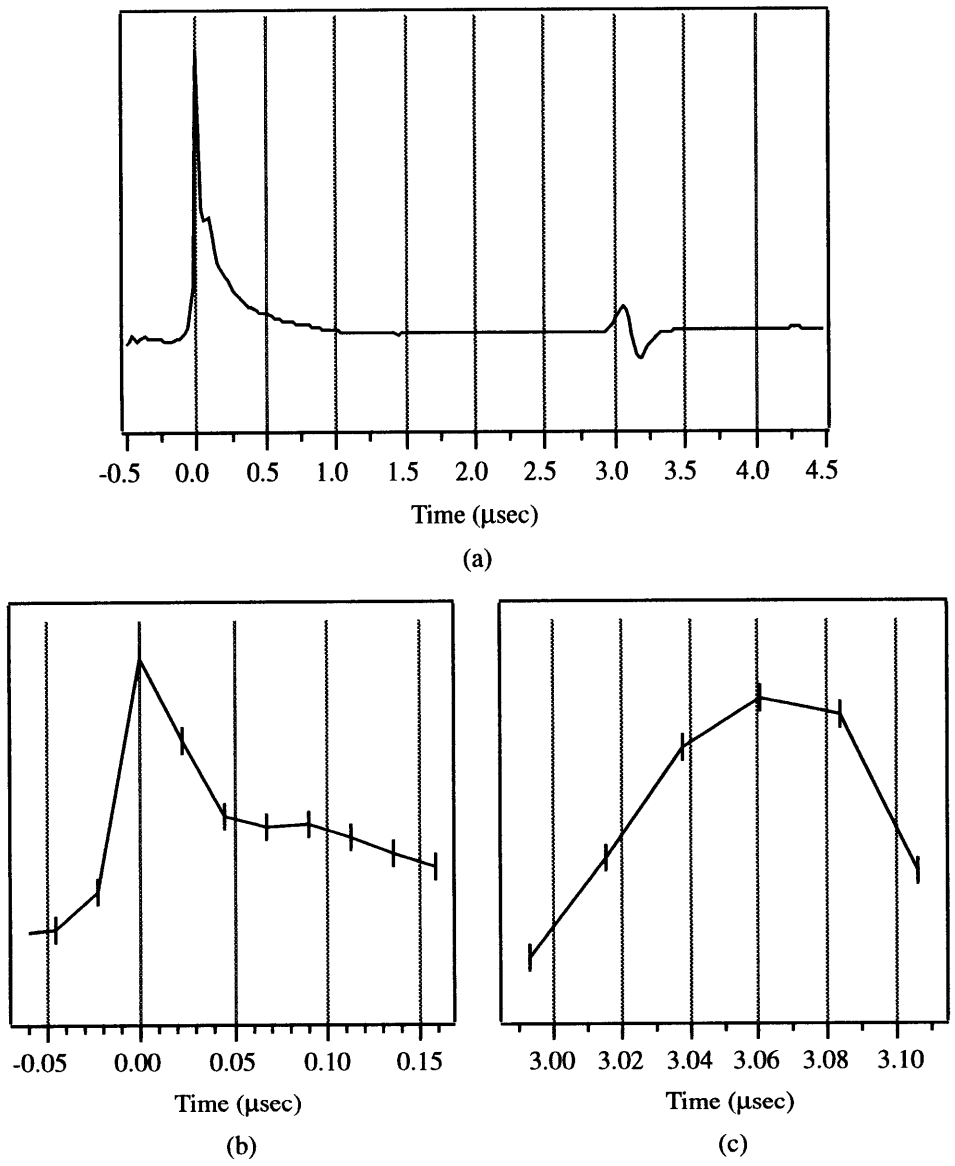

FIG. 7-4. An oscilloscope trace illustrating how it is discretely stored by the computer. (b) and (c) are blow-ups of the radiation spike and the peak of the Rayleigh pulse, respectively, showing the individual data points.

measurement made between two Rayleigh pulses would be subject to error around ±0.04μsec. (Later, when comparing experimental velocity results with published values, it will become evident that time measurements were probably even more accurate than conceded by these expected errors.)

7.3.3 Velocity error

The expected distance and time measurement errors then add to yield the probable error in the velocity calculation. As always, velocity is given by distance divided by time, or v=d/t, but when introducing errors to the quantities, the equation becomes

$$v \pm v_{error} = \frac{d \pm d_{error}}{t \pm t_{error}}. \tag{7-1}$$

Assuming the errors to be much smaller than the measured quantities themselves, the division can be approximated by normalizing the errors and adding them. Accordingly,

$$\frac{d \pm d_{error}}{t \pm t_{error}} = \frac{d}{t} \cdot \left(\frac{1 \pm \frac{d_{error}}{d}}{1 \pm \frac{t_{error}}{t}} \right) \approx \frac{d}{t} \cdot \left[1 \pm \left(\frac{d_{error}}{d} + \frac{t_{error}}{t} \right) \right]. \tag{7-2}$$

Thus, the normalized velocity error is very closely

$$\frac{v_{error}}{v} \approx \pm \left(\frac{d_{error}}{d} + \frac{t_{error}}{t} \right). \tag{7-3}$$

Note that since the distance and time measurement errors are constant for this particular experimental setup, the relative velocity error can be reduced by increasing the total distance between detection spot locations.

As an example, consider the previously discussed case regarding the aluminum sample. The array of detection locations spanned 10.16mm with a measured total time for the wave to travel by them of 3.43μsec. Merely from these two values, representing measurements taken for only the two extreme detection locations, the Rayleigh velocity is calculated at 2.962mm/μsec with an error of ±0.036mm/μsec. For this simplistic method of velocity calculation, the sizeable error seems justifiably necessary considering the previous argument.

However, as discussed earlier, there were not only two data points from which to determine the velocity. Instead, traces were gathered at numerous detection spot locations—anywhere from 9 to 15—and the velocity was calculated from the slope of a least-squares minimum line fit to the plotted data points. The Rayleigh velocity of the aluminum sample calculated in this way is 2.957mm/μsec. The possible error in the calculation is surely the same as before, but logically the probability of the real velocity being that far from the calculated value must be greatly reduced. In other words, the level of confidence that the real value lies within a more focused range is considerably higher than before. Of course, quantitative probabilities cannot be determined with the limited information provided by this experiment, but the qualitative understanding exists. Increasing the number of detection locations tightens the probability curve around the calculated velocity, but it does not affect the possibility of error.

8 RESULTS

Satisfying the immediate objective of this thesis, Rayleigh wave velocities of several bulk materials, including both isotropic and cubic crystalline samples, were measured to demonstrate the accuracy of this fully laser-based system. But beyond the elemental intent of velocity measurement, important qualitative and quantitative information was gathered concerning the effectiveness of generation mechanisms and source directionality. Where possible, the differences between thermoelastic and ablative generation were explored to better understand the realizable extent to which generating surface waves nondestructively with lasers is ultimately plausible. Also, to support the qualitative arguments made in Chapters 4 and 6, quantitative comparisons were made between point source and line source generation to show how source directivity improves the generation efficiency, in turn promoting the applicability of nondestructive thermoelastic generation in materials where it would otherwise have been undetectable.

8.1 Material Samples and Absorption

The tested isotropic samples consisted of 6061-T6 aluminum, 7075-T651 aluminum, and fused silica. Aluminum, like all metals, is extremely absorptive to 1.064 μm radiation, so a thermoelastically generated source would exist right beneath the sample's surface and would expectedly be very efficient. Metals provide excellent laser-ultrasonics test specimens because they are so remarkably absorptive to the high-energy infrared lasers, yet they reflect the wavelengths typical to visible detection lasers.

At the other extreme, fused silica, along with quartz and most other glasses, is almost completely transparent to the YAG laser beam. Only the impurities or imperfections of a fused silica sample could possibly permit even ablative generation to occur, thermoelastic generation being totally out of the question. Fused silica also reflects only about 3.5% of a He-Ne laser beam, so the total power input to the photodiode would be exceedingly low without any surface treatments.

Therefore, to assist in the generation and detection of surface waves on fused silica, two specimens were coated with aluminum films, one with 300 Å and the other with 2 μm. Since the generated Rayleigh pulses had widths on the order of 1 mm, the aluminum films were not anticipated to cause any appreciable change in the velocity. The propagating pulse would penetrate much deeper than the thickness of the films, expectedly at a velocity almost wholly determined by the properties of the fused silica. How the films would improve generation was not totally certain at the time, but surely the sample's reflectivity to the detection laser would be greatly increased.

Anisotropic specimens included (111)-cut gallium arsenide and silicon and (100)-cut germanium. These three cubic crystalline semi-conductors were chosen for their particular optical properties. Overall their absorption spectrums are very similar, but right in the vicinity of the YAG wavelength they have very different absorption characteristics. Each semi-conductor has a sharp cut-off around 1.064 μm. The absorption of gallium arsenide cuts off just before, representing transmission of the YAG wavelength. Germanium's absorption, at the other extreme, does not cut off until just after 1.064 μm, so it would behave more like a metal. Silicon's response, however, was not known beforehand because it's absorption cut-off is too close to 1.064 μm to really know whether it would absorb or transmit the YAG's energy.

All specimens were discs of 25.4 mm (1 in) in diameter, and their thicknesses varied from 3.18 to 12.7 mm (1/8 to 1/2 in).

8.2 Thermoelastic vs. Ablative Generation

It is very difficult to discuss the results of thermoelastic versus ablative generation without simultaneously comparing point source and line source generation because, ultimately, employing the cylindrical lens to line focus the excitation beam was what produced thermoelastically generated pulses strong enough to be distinguishable from the signal noise. For some specimens, though, whose absorption of the YAG wavelength was nonexistent, the line-focused beam was still not enough to produce detectable thermoelastically generated waves. Therefore, to express a clear understanding of the dependence of the wave amplitude on the input pulse energy and, thus, the generation mechanism, line source generation will be assumed. The advantages of using a line source over a point source will be discussed in detail in the following section.

8.2.1 In general

Figure 8-1 shows the effect of varying the input pulse energy on the signal amplitude of detected Rayleigh waves. This specific set of data points came from a test on aluminum, but it is included to illustrate the general differences between thermoelastic and ablative generation. As is characteristic with metals, the aluminum specimen efficiently absorbed all the YAG's energy just below the surface that was not initially reflected, and, in fact, the Rayleigh signal pulse could be distinguished at energies as low as 1 mJ. At pulse energies less than approximately 12–13 mJ, waves were excited thermoelastically without damage of any kind to the surface. The pulse shape was clean and symmetric, very close to the derivative of a Gaussian, which would be expectant of a monopolar pulse. The data points agree with the theory in Chapter 4 that the amplitude of thermoelastically generated waves is linearly dependent on the input energy.

At about 12 or 13 mJ, the specimen could not absorb any more energy, and the surface began to ablate. Instantly, the signal amplitude increased even though the energy had not been increased. From this alone it can be seen that ablative generation provided a more

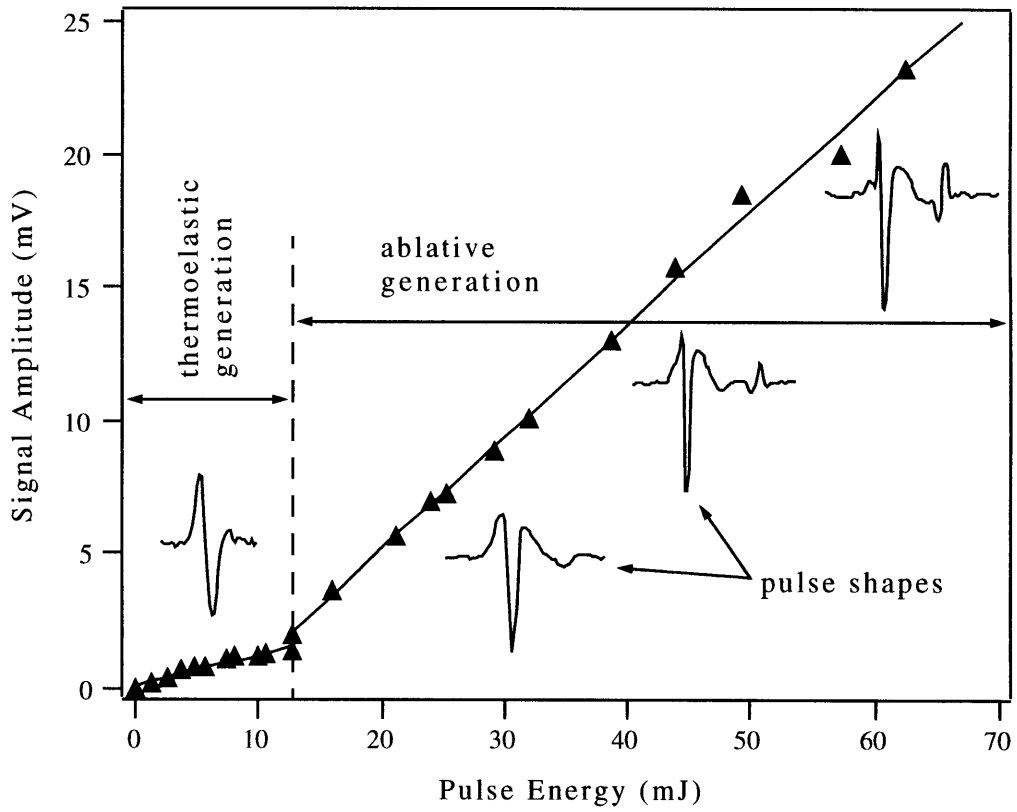

FIG. 8-1. Peak-to-peak signal amplitude as a function of the excitation laser pulse energy for an aluminum sample using a line-focused source. Note the increasing complexity of the received pulse shape as the generation mechanism gets increasingly violent.

efficient means of producing surface waves. As the energy was increased, the signal amplitude grew at a faster rate than it had in the thermoelastic regime. The data points seem to suggest a linear dependency, as was the case in the thermoelastic regime, but no theory thus far has given any reason to believe any such result. In general, the ablative mechanism is too destructive and unpredictable to theorize exactly how the amplitude depends on the energy. In fact, aluminum was the only material that did not suggest diminishing returns while increasing the pulse energy. Aluminum's apparently linear gain is left unexplained. In any case, ablative generation resulted in much more efficiently generated waves than thermoelastic generation, i.e. less energy was required to increase the signal amplitude an equivalent amount.

Another key point of comparison is the pulse shape itself. Remember that thermoelastic generation produced a smooth, symmetric pulse arising from the simple mechanism involved with the thermal expanding and contracting of the localized area. Ablation involves too many variables, including the changing of the surface with time, to be as well understood as that. Nonetheless, three pulse shapes are included in the ablative regime to show the increasing complexity of the received pulse shape as the generation mechanism got increasingly violent. Obviously, pulse shapes like these would be difficult to predict with simple models.

8.2.2 Material specific

With regards to each specific material, it is important to discuss whether thermoelastic generation was possible or not, and if so, what was the range? Basically, how did each specimen react to the excitation laser? The first specimen to be tested was gallium arsenide. Transmitting most of the nonreflected YAG beam, it failed to absorb enough energy to thermoelastically generate detectable surface waves. In fact, no signal pulse was observed until 24 mJ when the surface began to ablate. Waves became detectable on silicon also at 24 mJ, but the surface did not begin to ablate until after 35 mJ. Though the silicon specimen did transmit a substantial amount of the YAG beam, as expected, it allowed waves to be detected without causing permanent damage to the surface.

Nonetheless, the germanium and aluminum samples proved to be by far the best thermoelastic test specimens. On each of the samples, thermoelastically generated waves were detectable at energies as low as 1 mJ and upwards of 12 mJ where the ablation regime was entered. Velocity tests run at 7 or 8 mJ provided more than sufficient amplitude for excellent clarity and detail while staying well away from critical ablative energy densities.

Even with the aluminum films deposited on their surfaces, the fused silica samples were the most difficult to test, not because of detection, but because of not being able to deposit enough energy in the films to generate detectable waves. Thermoelastically generated

waves could barely be observed on the sample with 2 μm of aluminum, but they were not dependably distinguishable from the signal noise. Furthermore, the 300 Å film made no difference at all. Therefore, for generation purposes, the aluminum films served solely as catalysts for ablation to occur. Tests on both samples were run at energies in excess of 20 mJ with considerable damage to their surfaces.

8.3 Line Source vs. Point Source

Throughout this thesis, line source generation has been praised for its ability to direct the laser's energy, thus increasing the signal amplitude and ultimately requiring less energy. To give a better understanding of just how substantial the benefits of it are, two tests were run to quantitatively compare line source and point source generation. The first test comparatively measured the conversion of laser energy to acoustic energy while the second measured spatial attenuation. Both tests were done using the germanium sample.

8.3.1 Energy conversion

Figure 8-2 shows the results of the first test. The signal amplitudes of each method were measured for varying energy while holding the distance between the excitation and detection spots constant. Notice that the point source did not produce a detectable signal until ablation occurred at 4 mJ. On the other hand, thermoelastically generated waves were detectable using the line source well before then.

Overall, it is quite apparent that the line source produced considerably stronger waves than the point source, but this was not always the case. Between 7–12 mJ the waves ablatively produced by the point source were stronger than the waves thermoelastically produced by the line source, but that was to be expected. The violent generation mechanism produced by ablation is considerably more efficient than the thermal expansion produced by the absorption of laser energy. Still, though, the small increase in signal amplitude does not justify the surface damage incurred through ablation. The line source may not

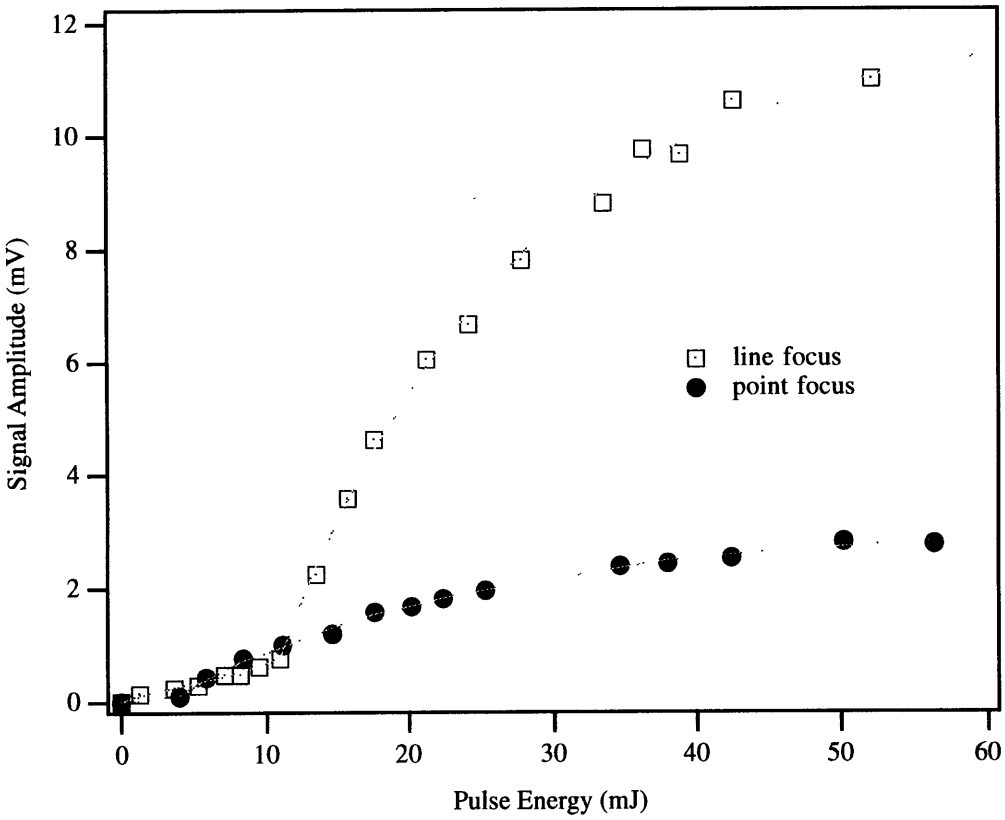

FIG. 8-2. Signal amplitude as a function of pulse energy to compare the conversion of laser energy to acoustic energy.

have converted more laser energy into acoustic energy at these levels, but the ability to thermoelastically generate the waves with comparable signal amplitude makes it superior.

A notable characteristic of these curves is the diminishing energy conversion in the ablative regime. Figure 8-1 showed aluminum to have a linear fit to the data, but for germanium the data seems to be exponential with an upper limit.

8.3.2 Spatial attenuation

Using a line source to direct the acoustic energy perpendicular to the line not only produces larger amplitude waves, but it also greatly reduces the attenuation of the waves as they travel away from the excitation spot. Waves generated by a point source propagate

outward equally in all directions, losing amplitude as they expand with a 1/r dependence. An infinite line source, however, produces waves that propagate without expanding, i.e. constant wave fronts that do not attenuate because of increasing size. The line source used here, of course, was not infinite, so it did radiate some energy in directions other than the normal axis, but still it resulted in considerably lesser attenuation.

Attenuation data for the germanium sample is shown in Figure 8-3. The signal amplitude was measured as a function of distance from the excitation spot while holding energy constant. Then, the data sets were plotted on a logarithmic amplitude scale, curve fit with lines, and normalized such that they both had equal amplitudes at the source to simulate similar initial conditions. The curve-fitted lines show the waves generated by the line

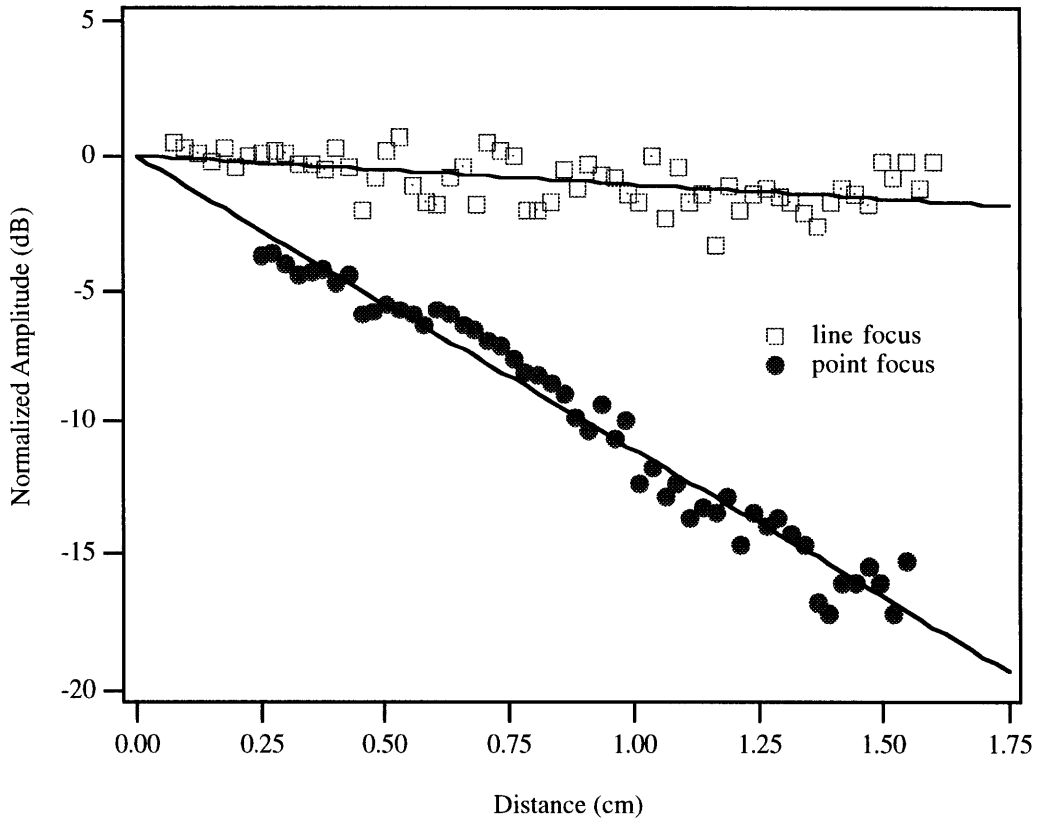

FIG. 8-3. Attenuation on germanium for both the line source and point source. The data and the curve-fitted lines have been normalized at the source to simulate similar initial conditions.

source to attenuate at 1 dB/cm, while the waves generated by the point source attenuated at over ten times that rate. Note that the variation in the detected signal amplitude is due mostly to varying surface reflectivity, not measurement error.

Undeniably, the lesser attenuation of the line source is beneficial in velocity measurements, where waves must be observed at a distance from the excitation source. Being able to detect waves close to the source does not necessarily mean that they can be seen further from the source where it is important. At a distance of 1 cm, a point source generated wave had only one tenth the amplitude of a wave generated by the line source. Of course, not all the attenuation associated with these methods is due to geometric considerations; the material itself has an inherent attenuation which is a function of frequency. Line source generation simply minimizes the total attenuation losses.

8.4 Measured Velocities

Demonstrating the accuracy of this technique to measure the surface wave velocity was, fortunately, independent of any of the situations discussed above. It was independent of generation mechanism, of pulse energy, of source shape and directivity. In other words, it did not matter how the waves were excited, only that they were. Using the procedure discussed in Chapter 7, the Rayleigh velocity was measured for each of the isotropic specimens and for specific crystal directions of each of the anisotropic semi-conductor specimens. Also, anisotropy curves were measured for germanium and silicon to demonstrate the angular dependence of the velocity.

8.4.1 Isotropic materials

The velocity results for the isotropic samples are given in Table 8-1. It is seen that the experimental values agree well with published data to within 1% except, of course for the 6061-T6 aluminum alloy. Tests were repeated again and again for that sample in various directions, consistently resulting in a velocity of 2.96 mm/μsec. Exactly why the measured velocity was so far from the published value is not known, but the Rayleigh wave

TABLE 8-1. Surface Wave Velocities of Various Isotropic Materials Comparing Experimental Results with Published Data

Substrate Material	Measured Wave Velocity (mm/μsec)	Published Wave Velocity (mm/μsec)
Fused silica w/300Å Al	3.40±0.04	3.40[a]
Fused silica w/2μm Al	3.41±0.03	3.40[a]
6061-T6 aluminum alloy	2.96±0.02	2.87[b]
7075-T651 aluminum alloy	2.90±0.04	2.88[b]

a. R. M. Arzt and K. Dransfelt, "Excitation of Rayleigh Waves at High Frequencies and at Low Temperatures," *Appl. Phys.* **6**, 157 (1965).

b. These velocities were calculated from material properties given in the *CRC Handbook of Material Science*, Charles T. Lynch, ed. (CRC Press, Inc., Cleveland, 1975), Volume II.

velocity of that particular sample strongly suggests that it may not have been the correct alloy.

By definition, the errors calculated using Eq. 7-3 suggest that repeated tests would result in velocities varying within a range defined by them. However, this technique demonstrated much better repeatability than the estimated errors defined by the logic of Chapter 7 had foreseen, for the measured velocities stayed well within a range of ±0.4% of their average, generally a factor of 2 or 3 better than anticipated.

8.4.2 Cubic crystals

Table 8-2 shows the velocity results of the anisotropic substrates for specific propagation directions. Comparison with published values shows even better accuracy for these single crystal specimens than for the isotropic specimens. The most likely explanation is that the natural molecular ordering of crystals results in more consistent material properties than do amorphous isotropic materials. All the results were accurate to within 0.2% of the expected values even though the estimated errors anticipated much less reliable accuracy. Furthermore, the results were repeatable within a range of ±0.1%.

TABLE 8-2. Surface Wave Velocities of Various Cubic Crystals Comparing Experimental Results with Published Data

Substrate Material and Prop. Direction	Measured Wave Velocity (mm/μsec)	Published Wave Velocity (mm/μsec)
Gallium arsenide [110] direction on (111) plane	2.430±0.020	2.428[a]
Gallium arsenide 30° from [110] on (111) plane	2.608±0.017	2.605[b]
Germanium [100] direction on (001) plane	2.939±0.023	2.934[b]
Silicon [110] direction on (111) plane	4.550±0.052	4.546[b]

a. Farnell, p. 136.

b. Auld, p. 381.

Anisotropy curves were gathered for germanium and silicon by measuring the surface wave velocities in directions beyond the specific crystal axes. Figure 8-4 shows the experimental results for silicon and compares them with the theoretical curve determined by Farnell. Only in the [110] direction were the surface waves of the Rayleigh-type, but the normal component of surface waves propagating in any direction could still be measured using the laser detection system.

The results for germanium are shown in Figure 8-5, but unlike with silicon, the theoretical anisotropy curve includes the existence of pseudosurface wave propagation. For germanium, only surface waves travelling in the [100] and [110] directions are of the Rayleigh-type, and only in those specific directions does surface wave propagation con-

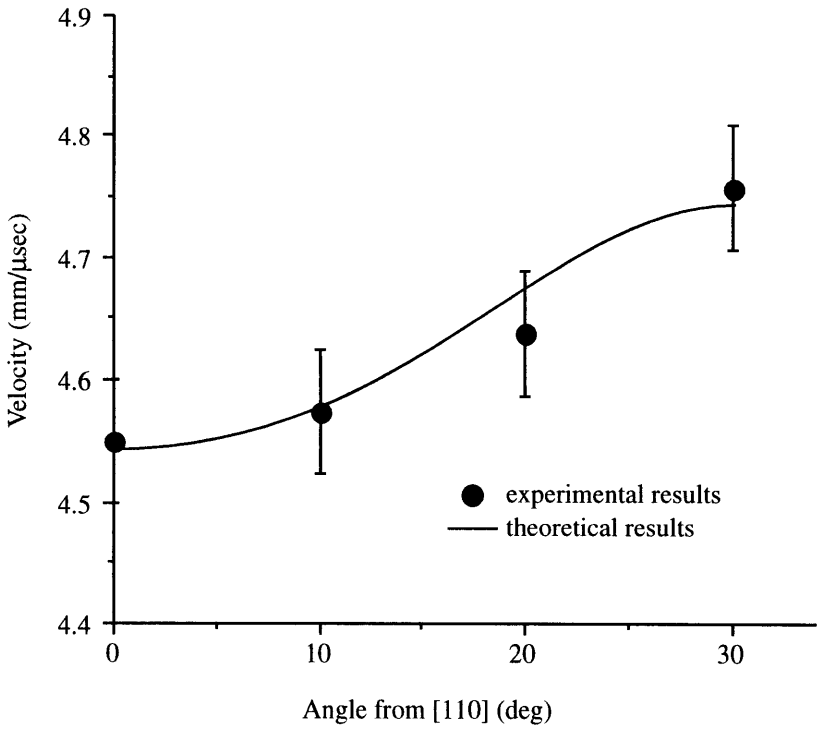

FIG. 8-4. Comparison of experimentally and theoretically obtained wave velocities for propagation on the (111) plane of silicon. Error bars indicate ~1.1% error in the experimental data.

sist of a single mode. In fact, in all other directions, the normal surface displacement is a combination of the normal surface, slow bulk shear, and pseudosurface waves, so the experimental data is only expected to coincide with the theoretical curve in the [100] and [110] directions.

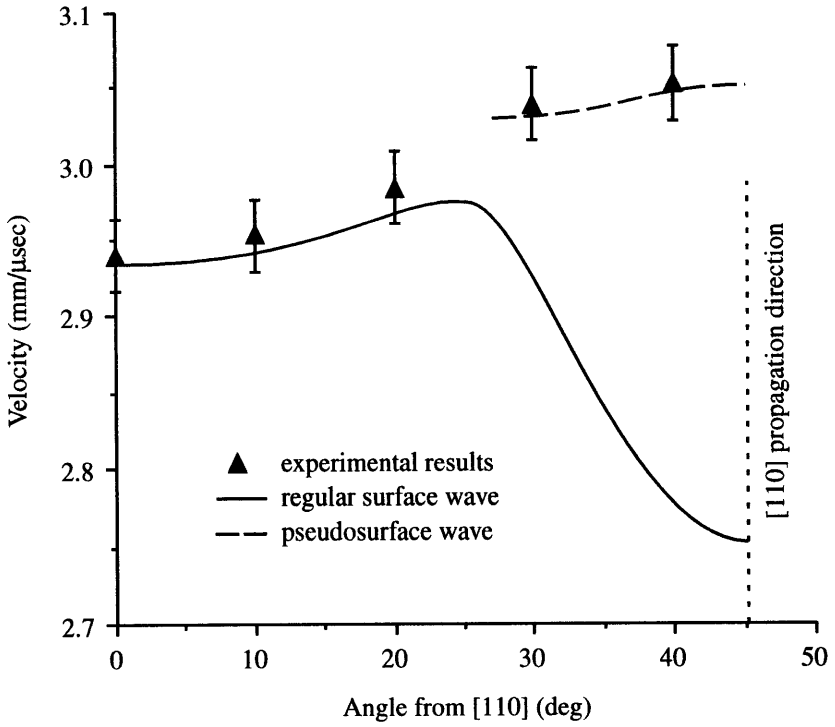

FIG. 8-5. Comparison of experimentally and theoretically obtained wave velocities for propagation on the (001) plane of germanium. Error bars indicate ~0.8% error in the experimental data.

9 CONCLUSION

9.1 Summary

Rayleigh wave velocities of several bulk material substrates were accurately measured using a system of lasers to both excite and detect the waves. The tests were done rapidly, remotely, and without the need for a coupling medium, thus surmounting many of the problems commonly associated with the use of piezoelectric transducers.

In most cases, the neodymium:YAG pulse laser used to excite the waves successfully generated them thermoelastically and without damage to the surface. This was made possible by line-focusing the beam with a cylindrical lens which directed the energy of the acoustic source in the direction of the detection probe. However, gallium arsenide and fused silica, which were very transmissive to the YAG wavelength, still required the waves to be generated ablatively for the detected signal to be distinguished from the signal noise. This, of course, resulted in permanent surface damage.

The He-Ne laser used to observe the propagation of the surface waves was configured using an optical beam deflection/knife-edge detection scheme. The system employed a micropositioning translation stage to accurately measure relative distances with a precision of $\pm 2.5\,\mu m$. Beam deflection systems are generally less sensitive than interferometry-based systems, but this particular setup was relatively inexpensive and easy to construct.

The experimental velocity results agreed with published values to well within 1%, except for the particularly questionable aluminum sample, demonstrating the validity of this

technique. Also the results were extremely reproducible within a range of approximately 0.2%. The precision of the technique was mostly limited by the resolution of the oscilloscope traces as they were digitally captured onto the computer, for the error incurred with the time measurements far exceeded the distance measurement error. It was explained in Chapter 7 how the limited resolution could logically be surpassed by interpolation techniques, thus greatly reducing the error, but an upgrade in the software or hardware would surely be more agreeable to the scientific community.

9.2 Future Application to Thin Films

The motivation of this research was the need for a novel technique to nondestructively measure the elastic properties of thin films, so it is important to discuss possible courses of action toward applying what was learned by this research to the material characterization of thin films. As already explained, the largest concern must be the development of a method of generating the waves at very high frequencies such that the Rayleigh waves penetrate to a depth less than the thickness of a given film. This is to insure that the velocity of the waves is wholly or in most part governed by the properties of the film alone. However, the knife-edge technique investigated here cannot detect frequencies much greater than 50 MHz, for the probe size is limited by diffraction and cannot practically be smaller than 10 μm. Thus, changes must be made to both generation and detection in order to measure the surface wave velocity of the film material.

9.2.1 Generation

It was stated earlier that the rise-time of the displacements produced by laser-generated waves are comparable to the laser rise-time, which for a Q-switched laser can be of the order of a few nanoseconds. Instead of using the usual pulsed laser time durations, though, Krautkramer[1] demonstrated the use of a mode-locked laser for generation which

1. J. Krautkramer, *9th World Conf.* NDT, Plenary Lecture, Melborne, Australia.

delivered picosecond pulses. The resultant acoustic pulses generated in steel had a width of only 2 nsec and a rise time of 1 nsec. Instead of switching out a single pulse from the usual train of pulses resulting from mode locking as he did, the train of pulses itself could be used to irradiate a solid to force generation at the repetition frequency of the mode-locked pulses. Brienza and DeMaria demonstrated this technique at a pulsing rate of 200 MHz and observed high harmonic content to 2 GHz, which indicated that their acoustic pulses had rise times significantly less than 1 nsec.[1]

Unfortunately, the pulsing rate of a mode-locked laser is determined by the optical circulation time of the laser cavity. The finite size of the laser cavity components, including the oscillator and amplifier crystals and the electro-optical elements associated with Q-switching and mode-locking, limits the pulsing rate to below 1 GHz, if even that. An alternative approach is presented by intensity modulated laser pulses, produced using intersecting beams frequency-shifted by Brilliouin scattering.[2] The modulated pulse would imitate a train of pulses and could be modulated at much higher frequencies.

Of course, thin films are typically less that a micron thick and would, therefore, require pulsing rates in excess of a few gigahertz. Further investigation would be necessary, though, to determine whether or not materials can actually react that fast thermally. If not, then generation will unfortunately have to be accomplished with conventional piezoelectric transducers which require direct contact to the specimen, a sacrifice which will have to be made.

9.2.2 Detection

No sacrifice will have to be made, though, in detection. The knife-edge technique and interferometry may not be applicable at very high frequencies, but deflection of the probing beam by surface grating diffraction, as described in Chapter 5, is perfect for continu-

1. M. J. Brienza and A. J. DeMaria, "Laser-Induced Microwave Sound by Surface Heating," *Appl. Phys. Lett.* **11**, 44-46 (1967).
2. Sherwin Amimoto, The Aerospace Corp., El Segundo, CA (verbal communication).

ous or tone-burst acoustic surface wave excitation. Slobodnik employed the diffraction grating technique to measure attenuation losses in $LiNbO_3$ at 1, 2, and 3 GHz.[1] A setup similar to his could easily be used to measure the velocity of surface waves in thin films.

9.2.3 Further Comments

A significantly different approach to measuring the elastic constants of thin films with surface waves was investigated by Kim and Achenbach.[2] Using a line focus acoustic microscope, they obtained dispersive velocity data by gathering velocity measurements for various film thicknesses and frequencies. The thin film elastic constants were obtained by seeking a least-squares minimum of the theoretical dispersion relation, as described elsewhere[3], as a function of the elastic constants for given wave velocity, film thickness, and frequency. The technique merits further investigation, for it does not require gigahertz frequencies, and it defines a method of calculating all three anisotropic elastic constants, but the results were extremely inaccurate, and the process required numerous samples instead of just one, which was a preferred fundamental requirement set by the motivation of this research.

1. Slobodnik, p. 95.
2. J. O. Kim and J. D. Achenbach, "Line Focus Acoustic Microscopy to Measure Anisotropic Acoustic Properties of Thin Films," *Thin Solid Films.* **214**, 25-34 (1992).
3. J. O. Kim, J. D. Achenbach, P. B. Mirkarimi, M. Shinn, and S. A. Barnett, submitted for publication.